Microscopic description of nuclear shapes and collective excitations

Lotina, Luka

UNIVERSITY OF ZAGREB
FACULTY OF SCIENCE
DEPARTMENT OF PHYSICS

Luka Lotina

MICROSCOPIC DESCRIPTION OF NUCLEAR SHAPES AND COLLECTIVE EXCITATIONS

Master Thesis

Zagreb, 2020

SVEUČILIŠTE U ZAGREBU
PRIRODOSLOVNO-MATEMATIČKI FAKULTET
FIZIČKI ODSJEK

Luka Lotina

MIKROSKOPSKI OPIS OBLIKA I KOLEKTIVNIH POBUĐENJA ATOMSKE JEZGRE

Diplomski rad

Zagreb, 2020

UNIVERSITY OF ZAGREB
FACULTY OF SCIENCE
DEPARTMENT OF PHYSICS

INTEGRATED UNDERGRADUATE AND GRADUATE UNIVERSITY
PROGRAMME IN PHYSICS

Luka Lotina

Master Thesis

Microscopic description of nuclear shapes and collective excitations

Advisor: Professor Kosuke Nomura, doc. dr. sc.

Master Thesis grade: _____

Committee: 1. _____

2. _____

3. _____

Master Thesis defence date: _____

Zagreb, 2020

I would like to thank my advisor, Professor Kosuke Nomura, for being a great advisor, for answering all the questions I asked, and for helping me understand this topic better and learn all the necessary skills. Without his help, this thesis would not have been successfully written. I would also like to thank Professor Tamara Nikšić for helping me learn how to run some of the required codes. Finally, I would like to thank my family and all my friends for their support.

Mikroskopski opis oblika i kolektivnih pobuđenja atomske jezgre

Sažetak

U ovom radu primijenjen je model srednjeg polja baziran na relativističkim energijskim funkcionalima gustoće (REDF) na parno-parne izotope kriptona, barija i ksenona. Pomoću relativističkog Hartree-Bogoliubovljevog (RHB) modela i DD-PC1 funkcionala, ispitane su kvadrupolne i oktupolne deformacije danih izotopa u osnovnom stanju. Oktupolne deformacije u osnovnom stanju izračunate su za jedan izotop kriptona, jedan izotop ksenona i sedam izotopa barija. Za izračun energija pobuđenja i snaga prijelaza korištena je metoda kvadrupolno-oktupolnog kolektivnog Hamiltonijana (QOCH). Izračunate energije pobuđenja i snage prijelaza uspoređene su s dostupnim eksperimentalnim podacima. Utvrđeno je da rezultati za teže jezgre, poput barija i ksenona, pokazuju puno bolje slaganje s eksperimentalnim podacima od rezultata za lakše jezgre kao što je kripton. Također je pokazano da su izračunate energije pobuđenja za stanja s pozitivnim paritetom u puno boljem slaganju s eksperimentalnim podacima od energija za stanja s negativnim paritetom.

Ključne riječi: kvadropolne deformacije, oktupolne deformacije, relativistički energijski funkcional gustoće, kvadrupolno-oktupolni kolektivni hamiltonijan

Microscopic description of nuclear shapes and collective excitations

Abstract

In this work, a mean-field model based on relativistic energy density functionals (REDF) was applied to even-even isotopes of krypton, barium and xenon. Quadrupole and octupole deformations of given isotopes in the ground-state were examined using a relativistic Hartree-Bogoliubov (RHB) model and a DD-PC1 functional. It was calculated that one krypton isotope, one xenon isotope and seven barium isotopes are octupole-deformed in the ground-state. A calculation of excitation energies and transition strengths was performed using a quadrupole-octupole collective Hamiltonian (QOCH). The results for the excitation energies and transition strengths were compared with the available experimental data. It is shown that the results for heavier nuclei, like barium and xenon, are in much better agreement with the experimental data than the results for lighter nuclei, like krypton. It is also shown that the calculated excitation energies of states with positive parity are in much better agreement with experimental data than energies of states with negative parity.

Keywords: quadrupole deformations, octupole deformations, relativistic energy density functional, quadrupole-octupole collective Hamiltonian

Contents

1 Introduction

The problem with describing the properties of a nucleus is that it is a many-body quantum system comprised of protons and neutrons which interact mainly via the nuclear force, which has a much more complicated form than the Coulomb force or gravity. In order to describe properties of a nucleus, models are developed that avoid explicitly modelling the nuclear force. According to the nuclear shell model, a nucleus might be viewed as a system of independent nucleons moving in an average potential [1]. The energies of nucleons are quantized and each nucleon fills a particular nuclear orbital (shell). Those nuclei that only have completely filled shells are more tightly bound than the neighbouring nuclei and are spherically shaped in the ground-state. If a nucleus is excited from the ground-state, or more nucleons are added, deformations of the spherical shape may occur due to long-range correlations between valence nucleons [2]. In this work, quadrupole and octupole shapes are examined. Nuclei with axially symmetric quadrupole deformations are characterized by an ellipsoidal shape, which can be prolate (rugby ball shape) or oblate (discus shape). Nuclei with octupole deformations are characterized by a pear-like shape. Octupole deformations are rarer and occur when there are interacting shells of opposite parity whose angular momentum differs by $3\hbar$ [3]. These interactions usually occur for nuclei with specific nucleon numbers, which will be discussed in the second chapter. The octuple deformation breaks reflection symmetry, and a nucleus with strong octupole deformation has large electric dipole and octupole transition strength. In particular, measurement of a very large E1 transition would imply the time-reversal (T) or Charge-Parity (CP) violation [4], and thus point to a testing ground for a new physics beyond the Standard Model of elementary particle physics in the context of low-energy nuclear physics. Given this general interest, the study of octupole shape is among the most prominent topics in nuclear physics, and the relevant experiments have been planned and already running at the radioactive-ion beams facilities around the world, e.g., at HIE-ISOLDE facility at CERN, Argonne National Laboratory, etc. Some of the recent experimental and theoretical advances in the research of octupole collectivity in nuclei can be found in [5, 6].

A model used in this work is a self-consistent mean field model (SCMF), where a nucleus is represented as a many-body system of independent nucleons moving

in a self-consistent potential that corresponds to the actual density distribution of a given nucleus [7–9]. SCMF model is analogous to Kohn-Sham density functional theory (DFT) [10], which describes a quantum many-body system in terms of a universal energy-density functional, effectively mapping a many-body problem onto a one-body problem [11]. The exact energy-density functional is approximated with powers and gradients of ground-state nucleon densities and is not necessarily related to any given nucleon-nucleon (NN) potential [11]. One of the most important classes of mean-field models are the relativistic mean-field (RMF) models which use a relativistic energy-density functional (REDF) to describe properties of a nucleus. A formalism of REDFs currently provides the most complete and precise theoretical framework for describing properties of the ground-state and collective excitations and is successfully applied to nuclei ranging from light to superheavy nuclei, from the nuclei in the valley of β-stability to the nuclei on the boundaries of the valley [12].

Mean-field models do not include pairing correlations that come into effect for nuclei with partially-filled shells. In order to fix this problem, a relativistic Hartree-Bogoliubov (RHB) model [9, 13] is used, a relativistic extension of the Hartree-Fock-Bogoliubov model, which takes into account these correlations. The RHB model provides a unified description of particle-hole (ph-) and particle-particle (pp-) correlations on a mean-field level by using two average potentials: the self-consistent mean-field potential and a pairing field [11]. Introducing Bogoliubov quasiparticle operators enables a ground state of a nucleus to be described by a Slater determinant that represents a vacuum with respect to independent quasiparticle operators. More detailed description of the RHB model will be given in the second chapter.

Another issue with the mean-field model is that a SCMF wave function necessarily breaks several symmetries of the nuclear Hamiltonian, e.g. translational and rotational. This means that the SCMF model alone cannot be used to compute excitation energy spectra and transition strengths between nuclear states. In order to compute them, a REDF framework has to be extended to take into account the restoration of broken symmetries and fluctuation of collective coordinates [13]. One of the most common methods used is the generator coordinate method (GCM) which uses RHB wave functions and weight functions to build the approximate eigenstates of the Hamiltonian of the nucleus. This method is very successful, but the calculations are very time-consuming. In this work, a REDF-based quadrupole-octupole Hamiltonian

(QOCH) [14, 15] is employed. In this method, vibrational and rotational kinetic energies are expressed in terms of the qadrupole and octupole deformation parameters β_2 and β_3 and the moments of inertia. The biggest advantage of this method, in comparison to GCM, is that the calculations are far less time-consuming, it takes only a few minutes for the QOCH calculations to finish. The QOCH method will also be discussed more in detail in the second chapter.

The octupole deformations in the rare-earth [16,17] to lanthanides ($Z \approx 56,\ N \approx 88$) [18, 19], and actinides ($Z \approx 88,\ N \approx 136$) [17, 20–23] regions are well studied both theoretically and experimentally. However, the regions with ($Z \approx 34,\ N \approx 34$), ($Z \approx 34,\ N \approx 56$), and ($Z \approx 56,\ N \approx 56$) have been much less explored theoretically. So, it is a principal aim of this work to address whether the theory predicts octupole deformation occurs in these mass regions as well. Furthermore, the evolution of deformations (quadrupole and octupole shapes, and shape coexistence) in the neutron-rich krypton isotopes is a theme of great interest, and has recently been extensively investigated by experiments such as at CERN [24] and RIKEN in Japan [25]. In this work, a DD-PC1 functional, in combination with the RHB model, was applied to even-even isotopes of krypton ($Z = 36,\ 30 \leq N \leq 66$), xenon ($Z = 54,\ 54 \leq N \leq 118$) and barium ($Z = 56,\ 54 \leq N \leq 98$). A potential energy surface (PES) was plotted in the β_2-β_3 plane and, for some of these isotopes, octupole deformations were observed. Special attention was given to isotopes with nucleon numbers for which static octupole deformations are expected. Low-lying excitation spectra, ground-state energies and transition strengths were calculated using the QOCH with parameters determined by SCMF calculations based on the DD-PC1 functional. The excitation energies were calculated for states up to $J^\pi = 7^-$ and the transition strengths were calculated for transitions between the first 1^-, 2^+ and 3^- states and the ground-state 0^+. All of the results were compared to the available experimental data, mostly found on the website of the National Nuclear Data Center (NNDC) [26].

This work is organised in the following way. In chapter 2, theoretical framework is explained. In the first subchapter, the theory behind quadrupole and octupole deformations is presented. The DFT, the RMF model with REDF and the QOCH are explained in the rest of the chapter. Results of the calculations are presented in chapter 3. PES is plotted in the $\beta_2 - \beta_3$ plane and static octupole deformations in the ground-state are shown for certain isotopes of krypton, xenon and barium.

Binding energy per nucleon number is plotted as a function of the neutron number for all three elements and the results are compared with experimental data. In the rest of the chapter, excitation energies and transition strengths are also plotted as a function of the neutron number and the results are also compared with the available experimental data. The last chapter contains the summary of the results and the outlook.

2 Theoretical framework

2.1 Quadrupole and octupole deformations

In order to describe nuclear deformations, the surface of the nucleus needs to be parameterized in some way. One possibility is to describe it by the length of the radius vector, which can be expanded in terms of a spherical harmonic expansion [3]

$$R(\theta,\phi) = c(\alpha)R_0\left[1+\sum_{\lambda=2}^{\lambda_{max}}\sum_{\mu=-\lambda}^{+\lambda}\alpha_{\lambda\mu}Y^*_{\lambda\mu}(\theta,\phi)\right]. \tag{2.1}$$

Deformation parameters $\alpha_{\lambda\mu}$ describe the length of the vector pointing from the origin to the surface, R_0 is the radius of a sphere with the same volume and $c(\alpha)$ is determined from the volume conservation condition. Since the radius needs to be real, this leads to a condition

$$(\alpha_{\lambda\mu})^* = (-1)^\mu\alpha_{\lambda-\mu}. \tag{2.2}$$

For $\lambda = 1$, three dipole deformation parameters $\alpha_{1\pm1}$, α_{10} are given by fixing a center of mass (c.m.) at the origin of the body-fixed frame, which leads to a condition

$$\int_V \mathbf{r}d^3\mathbf{r} = 0, \tag{2.3}$$

where V represents the volume of the enclosed surface in Eq. (2.1).

Parameters with $\lambda = 2$ represent quadrupole and parameters with $\lambda = 3$ represent octupole deformations. Including more deformations in the expansion in Eq. (2.1) leads to a more complicated picture with many deformation parameters. If quadrupole and octupole deformations are included, there are two independent quadrupole deformation parameters and seven octupole deformation parameters. However, when examining axially-symmetric nuclei, the picture is simplified because all $\mu \neq 0$ parameters vanish. The non-vanishing deformation parameters $\alpha_{\lambda0}$ are usually called β_λ.

Octupole deformations occur when there are ph-interactions between shells $(l+3, j+3)$ and (l, j) of opposite parity. These deformations are expected for nucleon numbers 34($g_{\frac{9}{2}} \leftrightarrow p_{\frac{3}{2}}$ coupling), 56($h_{\frac{11}{2}} \leftrightarrow d_{\frac{5}{2}}$ coupling), 88($i_{\frac{13}{2}} \leftrightarrow f_{\frac{7}{2}}$ coupling) and 134($j_{\frac{15}{2}} \leftrightarrow g_{\frac{9}{2}}$ coupling) [3], as is shown in Fig. 2.1. Nuclear deformations have

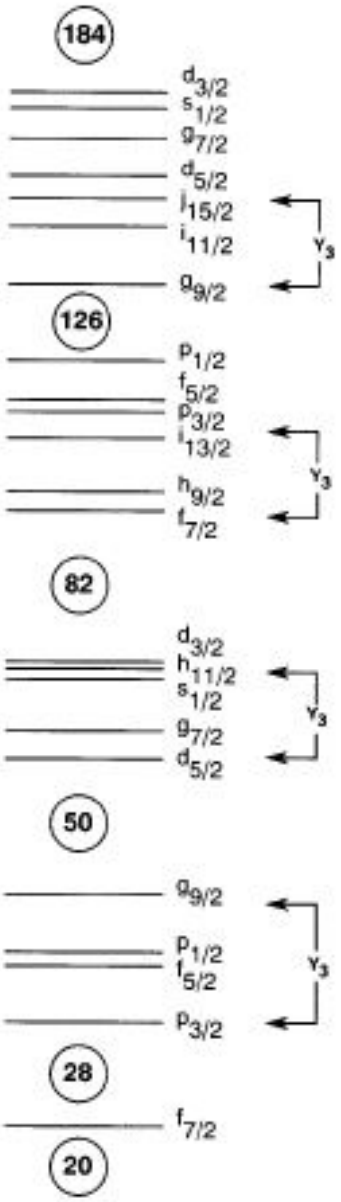

Figure 2.1: Nuclear spherical single-particle levels with indicated octupole couplings. The figure is taken from [3].

an effect on the low-lying excitation spectra. Lowering of the 2^+ state is characteristic for quadrupole deformations [1]. For nuclei with octupole deformations, odd-parity states 1^- and 3^- states exist in the low-lying excitation spectra, with transition strengths $B(E1)$ and $B(E3)$ from those states to the ground-state 0^+. The values for $B(E1)$ are usually $< 10^{-2}$ Weiskopff units (W.u.). The transition strengths $B(E3)$ can be > 10 W.u., and are easier to observe. In recent years, octupole deformations were confirmed in ^{224}Ra by successfully measuring $B(E3; 3^- \rightarrow 0^+)$ transition strength [2].

2.2 Density functional theory (DFT)

The basic concept of the DFT in nuclear physics is that the ground-state properties of the nucleus can be represented in terms of the ground-state density alone. This way, solving a Schrödinger equation with 3N coordinates is avoided, because the density $\rho(\mathbf{r})$ depends only on three spatial coordinates. This enables the DFT to be applied to large systems, such as heavy and superheavy nuclei, which makes it one of the most successful methods in nuclear physics. Most applications of the DFT use the effective single-particle Kohn-Sham (KS) equations [10]. The Hohenberg-Kohn theorem [27] states that there is a unique energy functional

$$E_s[\rho] = T_s[\rho] + \int d^3r \, v_s(\mathbf{r})\rho(\mathbf{r}) \tag{2.4}$$

for which the variational equation yields the exact ground state density $\rho_s(\mathbf{r})$. $T_s(\rho)$ is the universal kinetic energy functional of the non-interacting system and $v_s(\mathbf{r})$ is a unique local single-particle potential. According to the KS scheme, this potential is unique for every interacting system and is such that the exact ground-state density equals the ground-state density of the auxiliary non-interacting system:

$$\rho(\mathbf{r}) = \rho_s(\mathbf{r}) = \sum_i^N |\phi_i(\mathbf{r})|^2 , \tag{2.5}$$

where $\phi_i(\mathbf{r})$ represent wave-functions for N lowest occupied single-particle orbitals that satisfy the KS equations:

$$[-\nabla^2/2m + v_s(\mathbf{r})]\phi_i(\mathbf{r}) = \epsilon_i\phi_i(\mathbf{r}). \tag{2.6}$$

For a bound system, like the nucleus, the energy functional can be written as a sum of three separate functionals

$$F[\rho] = T_s[\rho] + E_H[\rho] + E_{xc}[\rho], \tag{2.7}$$

where T_s is a kinetic energy functional of a non-interacting system, E_H is a Hartree energy functional and E_{xc} is an exchange-correlation energy functional. The latter contains all other many-body effects. The local exchange potential is defined by the

relation:

$$v_{xc}[\rho](\mathbf{r}) = \frac{\delta E_{xc}[\rho]}{\delta \rho(\mathbf{r})}. \tag{2.8}$$

This way, the potential $v_s[\rho](\mathbf{r})$ can be written as

$$v_s[\rho](\mathbf{r}) = v_H[\rho](\mathbf{r}) + v_{xc}[\rho](\mathbf{r}). \tag{2.9}$$

The effective potential depends on the ground-state density, so equations (2.5), (2.6) and (2.9) need to be solved self-consistently and this is the KS scheme. The effectiveness of the KS scheme depends on the ability to construct a universal exchange-correlation energy functional E_{xc}. One approach is to construct E_{xc} from the first principles by incorporating exact constraints. The other approach is empirical, where parameters of the functional are optimized by fitting them to empirical data. The latter approach is the one used in constructing REDFs.

2.3 Relativistic mean-field model (RMF)

Most relativistic models in nuclear physics view a nucleus as a system of Dirac particles that interact via the meson- and photon-exchange. The minimal set of meson fields that is necessary to build the RMF model includes the isoscalar-scalar σ meson, the isoscalar-vector ω meson and the isovector-vector ρ meson [11]. There are many advantages to using a relativistic model than a non-relativistic one. For start, relativistic models include the nucleon spin degree of freedom, so the resulting nuclear spin-orbit potential emerges automatically. Also, RMF models enable a unique parameterization of nucleon currents and other time-odd components of the nuclear mean-field and they offer an explanation for phenomena like the empirical pseudospin symmetry [28]. In this work, the REDF used is the one constructed by adjusting parameters to empirical data on nuclear ground-states.

In the Dirac spinor field ψ, nucleon densities and currents are bilinear in that field

$$\bar{\psi}\mathcal{O}_\tau\Gamma\psi, \;\; \mathcal{O}_\tau \in \{1, \tau_i\}, \;\; \Gamma \in \{1, \gamma_\mu, \gamma_5, \gamma_5\gamma_\mu, \sigma_{\mu\nu}\}. \tag{2.10}$$

Operators τ_i represent isospin Pauli matrices and operators Γ represent Dirac matrices. In order to calculate the ground-state density and energy, relativistic linear single-nucleon KS equations need to be solved. These equations can be derived by

constructing an interaction Langrangian with four-fermion interaction terms: isoscalar-scalar: $(\bar{\psi}\psi)^2$, isoscalar-vector: $(\bar{\psi}\gamma_\mu\psi)(\bar{\psi}\gamma^\mu\psi)$, isovector-scalar: $(\bar{\psi}\vec{\tau}\psi)\cdot(\bar{\psi}\vec{\tau}\psi)$ and isovector-vector:$(\bar{\psi}\vec{\tau}\gamma_\mu\psi)\cdot(\bar{\psi}\vec{\tau}\gamma^\mu\psi)$, where arrows are used to denote vectors in isospin space. Vectors in coordinate space will be denoted with bold letters. A general Lagrangian could be written as a power series in the currents $\bar{\psi}\mathcal{O}\Gamma\psi$ and their derivatives, where higher-order terms represent in-medium many-body correlations. However, experimental data can constrain only a small number of parameters. Because of this, an effective Lagrangian containing only second-order interaction terms can be constructed. Analogous to meson exchange RMF phenomenology, in which the minimal set is built using σ, ω and ρ meson, an effective Lagrangian that includes isoscalar-scalar, isoscalar-vector and isovector-vector four-fermion interactions can be constructed and written in the following form:

$$\begin{aligned}\mathcal{L} =&\bar{\psi}(i\gamma\cdot\partial - m)\psi \\ &- \frac{1}{2}\alpha_S(\hat{\rho})(\bar{\psi}\psi)(\bar{\psi}\psi) - \frac{1}{2}\alpha_V(\hat{\rho})(\bar{\psi}\gamma^\mu\psi)(\bar{\psi}\gamma_\mu\psi) - \frac{1}{2}\alpha_{TV}(\hat{\rho})(\bar{\psi}\vec{\tau}\gamma^\mu\psi)(\bar{\psi}\vec{\tau}\gamma_\mu\psi) \\ &- \frac{1}{2}\delta_S(\partial_\nu\bar{\psi}\psi)(\partial^\nu\bar{\psi}\psi) - e\bar{\psi}\gamma\cdot A\frac{(1-\tau_3)}{2}\psi.\end{aligned} \tag{2.11}$$

What can be seen in Eq. (2.11) is that the Lagrangian, aside from the free-nucleon term and the point-coupling interaction terms, also includes the coupling of protons to the electromagnetic field. The derivative term in the equation takes into consideration finite-range interactions that are necessary for a quantitative description of nuclear density distribution, e.g. radii [11]. Similar interactions can be included in each space-isospin channel, but in practice only a single derivative term is constrained by the experimental data, and it is the one in isoscalar-scalar channel, which is consistent with conventional meson-exchange RMF models, in which the mass of the σ meson is adjusted to nuclear matter and ground-state properties of finite nuclei [11], while the values for the masses of the ω and ρ mesons are free. Also, in order to reduce the number of parameters, the isovector-scalar channel is left out of the REDF.

Strength parameters α_S, α_V and α_{TV} from the Eq. (2.11) are functions of the nucleon 4-current:

$$j^\mu = \bar{\psi}\gamma^\mu\psi = \hat{\rho}u^\mu, \tag{2.12}$$

where u^μ represents a 4-velocity defined by the relation $(1-\boldsymbol{v}^{-1/2})(1,\boldsymbol{v})$. In the rest-frame of the homogeneous nuclear matter $\boldsymbol{v}=0$ By varying the Lagrangian with respect to $\bar{\psi}$, the relativistic analogue to KS equation, called the single-nucleon Dirac equation, is obtained:

$$\left[\gamma_\mu(i\partial^\mu-\Sigma^\mu-\Sigma_R^\mu)-(m+\Sigma_S)\right]\psi=0, \tag{2.13}$$

where Σ^μ, Σ_R^μ, Σ_S and Σ_{TV}^μ are nucleon self-energies defined as:

$$\Sigma^\mu=\alpha_V(\rho_v)j^\mu+e\frac{1-\tau_3}{2}A^\mu \tag{2.14}$$

$$\Sigma_R^\mu=\frac{1}{2}\frac{j^\mu}{\rho_v}\left\{\frac{\partial\alpha_S}{\partial\rho}\rho_s^2+\frac{\partial\alpha_V}{\partial\rho}j_\mu j^\mu+\frac{\partial\alpha_{TV}}{\partial\rho}\vec{j}_\mu\vec{j}^\mu\right\} \tag{2.15}$$

$$\Sigma_S=\alpha_S(\rho_v)\rho_s-\delta_S\Box\rho_s \tag{2.16}$$

$$\Sigma_{TV}^\mu=\alpha_{TV}(\rho_v)\vec{j}^\mu. \tag{2.17}$$

Energies Σ_S, Σ^μ and Σ_{TV}^μ are isoscalar-scalar, isoscalar-vector and isovector-vector nucleon self-energies and Σ_R^μ is a term that arises by varying strength parameters with respect to the density operator. The isosclarar 4-current j_μ, the isovector 4-current $\vec{j}_\mu$ and the scalar density ρ_s are defined as expectation values of the following operators in the ground-state $|\phi_0\rangle$:

$$j_\mu=\left\langle\phi_0\left|\bar{\psi}\gamma_\mu\psi\right|\phi_0\right\rangle=\sum_k v_k^2\bar{\psi}_k\gamma_\mu\psi_k \tag{2.18}$$

$$\vec{j}^\mu=\left\langle\phi_0\left|\bar{\psi}\gamma_\mu\vec{\tau}\psi\right|\phi_0\right\rangle=\sum_k v_k^2\bar{\psi}_k\gamma_\mu\vec{\tau}\psi_k \tag{2.19}$$

$$\rho_s=\left\langle\phi_0\left|\bar{\psi}\psi\right|\phi_0\right\rangle=\sum_k v_k^2\bar{\psi}_k\psi_k. \tag{2.20}$$

Density ρ_v is the zeroth component of the 4-current j_μ. Wave function ψ_k is the Dirac spinor and the summation runs over occupied positive-energy single-nucleon orbitals, with v_k^2 representing occupation factors. This is called a "no-sea" approx-

imation where contributions of negative-energy solutions to currents and densities are omitted and the vacuum polarization effects are implicitly included in the adjustable density parameters of the theory. Equations (2.13)-(2.20) are solved self-consistently by iteration. A form of potentials in Eq. 2.13 is assumed. By solving the equation, single-particle wave functions are constructed. These wave functions are used in equations (2.18)-(2.20) to construct a new set of potentials. The procedure is repeated until the convergence happens. From the results, a total energy of the system [12]

$$E = \int \mathcal{H} \mathrm{d}\mathbf{r} \tag{2.21}$$

can be calculated, where $\mathcal{H}$ represents the Hamiltonian density, a (0,0) component of the impulse and energy tensor:

$$\mathcal{H} = T^{00} = \frac{\partial \mathcal{L}}{\partial \dot{\bar{\psi}}} \dot{\psi} - \mathcal{L}. \tag{2.22}$$

Strength parameters are parameterized in the following way:

$$\alpha_S(\rho) = a_S + (b_S + c_S x) e^{-d_S x} \tag{2.23}$$

$$\alpha_V(\rho) = a_V + b_V e^{-d_V x} \tag{2.24}$$

$$\alpha_{TV}(\rho) = b_{TV} e^{-d_{TV} x}, \tag{2.25}$$

where $x = \rho/\rho_{sat}$ and ρ_{sat} is the nucleon density at saturation in symmetric nuclear matter. Together, these 9 parameters are used to construct a DD-PC1 functional. These parameters are adjusted to experimental data on binding energies for different nuclei [29].

2.4 Relativistic Hartree-Bogoliubov (RHB) model

As was said earlier in the Introduction, the RMF model does not take into account pairing correlations, that play an important role in the description of open-shell nuclei. One way to incorporate pairing correlations into RMF model is by using a Bardeen-Cooper-Schrieffer (BCS) approximation, or a Hartree-Fock-Bogoliubov (HFB)

model. The HFB model is a generalization of the BCS approximation that includes the description of long-ranged ph- and short-ranged pp-correlations on the mean-field level. In order to construct the HFB model, a concept of Bogoliubov quasi-particle needs to be introduced. Quasiparticle operators β are defined by a unitary Bogoliubov transformation of the single-nucleon creation and annihilation operators $c^\dagger$ and c :

$$\beta_k^\dagger = \sum_l (U_{lk} c_l^\dagger + V_{lk} c_l). \tag{2.26}$$

The sum runs over the entire configuration space. The operator β_k is given by the Hermitian conjugation of Eq. (2.26). A generalized Bogoliubov transformation can be written in a matrix form:

$$\begin{pmatrix} \beta \\ \beta^\dagger \end{pmatrix} = \begin{pmatrix} U^\dagger & V^\dagger \\ V^T & U^T \end{pmatrix} \begin{pmatrix} c \\ c^\dagger \end{pmatrix} = \mathcal{W}^\dagger \begin{pmatrix} c \\ c^\dagger \end{pmatrix}. \tag{2.27}$$

In order for $\beta_k^\dagger$ and β_k to satisfy standard fermion commutation relations, the $\mathcal{W}$ matrix:

$$\mathcal{W} = \begin{pmatrix} U & V^* \\ V & U^* \end{pmatrix} \tag{2.28}$$

needs to be unitary. The ground-state of a nucleus $|\Phi\rangle$ is represented by a quasiparticle vacuum that satisfies the condition:

$$\beta_k |\Phi\rangle = 0 \tag{2.29}$$

for every k in the configuration space. A function that satisfies the condition from Eq. (2.29), for a given set of quasiparticle operators, is called a HFB wave function. The density matrix ρ and the pairing tensor κ are defined as:

$$\rho_{lk} = \left\langle \Phi \left| c_k^\dagger c_l \right| \Phi \right\rangle = (V^* V^T)_{lk} = \rho_{kl}^* \tag{2.30}$$

$$\kappa_{lk} = \langle \Phi | c_k c_l | \Phi \rangle = (V^* U^T)_{lk} = -\kappa_{kl}. \tag{2.31}$$

The energy density functional $E[\rho, \kappa, \kappa^*]$ is defined as an expectation value of a Hamiltonian in the ground-state of a nucleus:

$$\left\langle \Phi \left| \hat{H} \right| \Phi \right\rangle . \tag{2.32}$$

By varying the energy density functional with respect to ρ, κ and κ^*, a single-particle HFB equations can be obtained:

$$\begin{pmatrix} h - \lambda & \Delta \\ -\Delta^* & -h^* + \lambda \end{pmatrix} \begin{pmatrix} U_k \\ V_k \end{pmatrix} = e_k \begin{pmatrix} U_k \\ V_k \end{pmatrix}, \tag{2.33}$$

where h represents a Hartree-Fock Hamiltonian:

$$h_{lk}[\rho, \kappa, \kappa^*] = \frac{\partial E[\rho, \kappa, \kappa^*]}{\partial \rho_{kl}} \tag{2.34}$$

and Δ represents a pairing field:

$$\Delta_{lk}[\rho, \kappa] = \frac{\partial E[\rho, \kappa, \kappa^*]}{\partial \kappa^*_{lk}}. \tag{2.35}$$

The quasiparticle vacuum is not an eigenstate of the particle number operator, which means that in the HFB formalism, the number of particles is not conserved. For that reason, Eq. (2.33) contains a chemical potential λ, which can be determined from the condition that the expectation value of the particle number operator in the ground-state equals the total number of particles in the system.

The RHB model represents a relativistic extension of the HFB formalism. RHB equations can be written in the following form:

$$\begin{pmatrix} h_D - m - \lambda & \Delta \\ -\Delta^* & -h_D + m + \lambda \end{pmatrix} \begin{pmatrix} U_k(\mathbf{r}) \\ V_k(\mathbf{r}) \end{pmatrix} = e_k \begin{pmatrix} U_k \mathbf{r} \\ V_k(\mathbf{r}) \end{pmatrix}, \tag{2.36}$$

where h_D is a single-nucleon Dirac Hamiltonian from the Eq. 2.13, m is a mass of a nucleon and Δ is a pairing field.

Since there is no experimental evidence on relativistic effects in pairing correlations, a model of RHB with a non-relativistic pairing field can be employed. A general

relativistic two-body pairing field can be written as:

$$\hat{\Delta}_{a_1p_1,a_2p_2} = \frac{1}{2} \sum_{a_3p_3,a_4p_4} \langle a_1p_1, a_2p_2|V^{pp}|a_3p_3, a_4p_4\rangle \kappa_{a_3p_3,a_4p_4}, \tag{2.37}$$

where $p_1, p_2, p_3, p_4 = f, g$ are indices that refer to large and small components of the quasiparticle Dirac spinors:

$$U(\mathbf{r}, s, t) = \begin{pmatrix} f_U(\mathbf{r}, s, t) \\ ig_U(\mathbf{r}, s, t) \end{pmatrix},\ V(\mathbf{r}, s, t) = \begin{pmatrix} f_V(\mathbf{r}, s, t) \\ ig_V(\mathbf{r}, s, t) \end{pmatrix}, \tag{2.38}$$

with s and t representing spin and isospin. An approximation is used that takes into account only large components of spinors $U_k(\mathbf{r})$ and $V_k(\mathbf{r})$ when building a non-relativistic pairing tensor $\hat{\kappa}$. The pairing field can then be written as:

$$\hat{\Delta}_{ff} = \hat{\Delta}_{a_1f,a_2f} = \frac{1}{2} \sum_{a_3f,a_4f} \langle a_1f, a_2f\,|V^{pp}|\,a_3f, a_4f\rangle\, \kappa_{a_3f,a_4f}, \tag{2.39}$$

while other components $\hat{\Delta}_{fg}$, $\hat{\Delta}_{gf}$, $\hat{\Delta}_{gg}$ are omitted. In the pp-channel, interaction can be described by using the Gogny force:

$$V^{pp}(1,2) = \sum_{i=1,2} e^{-((\mathbf{r_1}-\mathbf{r_2})/\mu_i)^2}(W_i + B_iP^\sigma - H_iP^\tau - M_iP^\sigma P^\tau), \tag{2.40}$$

with a set of parameters μ_i, W_i, B_i, H_i and M_i ($i = 1, 2$) determined from the D1S parameterization [30]. An advantage of this method is that the Gogny force has a finite range, but the problem is that solving equations (2.36) can be very time-consuming.

Another way to describe the pairing field is to introduce a form of the pairing force that is separable in the momentum space and completely determined by two parameters that are adjusted to reproduce pairing properties of the Gogny force in nuclear matter [29]. The pairing gap in the singlet $^1\mathrm{S}_0$ channel can be written as:

$$\Delta(k) = -\int_0^\infty \frac{k'^2dk'}{2\pi^2} \left\langle k \left| V^{^1\mathrm{S}_0} \right| k' \right\rangle \frac{\Delta(k')}{2E(k')}. \tag{2.41}$$

Since the force is separable in the momentum space, the expectation value of the

potential can be written as:

$$\left\langle k \left| V^{^1\mathrm{S}_0} \right| k' \right\rangle = -Gp(k)p(k'), \tag{2.42}$$

where $p(k)$ is assumed to have a Gaussian form $p(k) = e^{-a^2k^2}$, with two parameters G and a determined from D1S parameterization [30]. The Eq. (2.42) can be transferred from the momentum space to the coordinate space:

$$V(\mathbf{r}_1, \mathbf{r}_2, \mathbf{r'}_1, \mathbf{r'}_2) = G\delta(\mathbf{R} - \mathbf{R'}P(\mathbf{r})P(\mathbf{r'})\frac{1}{2}(1 - P^\sigma)), \tag{2.43}$$

where $\mathbf{R} = \frac{1}{2}(\mathbf{r}_1 + \mathbf{r}_2)$ and $\mathbf{r} = \mathbf{r}_1 - \mathbf{r}_2$ are center of mass and relative coordinates. $P(\mathbf{r})$ is the Fourier transform of $p(k)$:

$$P(\mathbf{r}) = \frac{1}{(4\pi a^2)^{3/2}} e^{-\mathbf{r}^2/4a^2}. \tag{2.44}$$

The factor $\delta(\mathbf{R} - \mathbf{R}')$ preserves translational invariance.

Equations 2.36 can be solved by expanding the nucleon spinors $U(\mathbf{r}, s, t)$ and $V(\mathbf{r}, s, t)$ in the basis of a 3D harmonic oscillator (HO) in Cartesian coordinates [29]. Since axial symmetry is assumed in this work, equations 2.36 can be solved in cylindrical coordinates [12, 31]. This will be done in Appendix A.

By solving RHB equations in the previously described way, only a local minimum on the energy surface can be calculated. In order to calculate the energy as a function of the collective coordinate q, a constraint on the expectation value of a given operator needs to be imposed. A wave function $|\phi(q)\rangle$ needs to be constructed so that the total energy is minimized and that an operator $\hat{Q}$ has a fixed expectation value $q = \left\langle \Phi \left| \hat{Q} \right| \Phi \right\rangle$. This can be done by using a quadratic constraint method that uses a variation:

$$\langle H \rangle + \frac{C}{2} \left(\left\langle \hat{Q} \right\rangle - q \right)^2, \tag{2.45}$$

where $\langle H \rangle$ represents a total energy, $\left\langle \hat{Q} \right\rangle$ is an expectation value of a quadrupole or octupole operator, q is the constrained value of the multiple moment and C is the stiffness constant. In this way, the plotting of the potential energy surface in the $\beta_2 - \beta_3$ deformation plane is enabled.

2.5 Quadrupole-octupole collective Hamiltonian (QOCH)

Since mean-field models break certain symmetries, e.g. translational and rotational, other methods need to be combined with those models, so that low-lying excitation spectra and transition rates can be calculated. One of the commonly used methods is the generating coordinate method (GCM) [13], but using that method can lead to very time-consuming calculations. In this work, a quadropole-octupole collective Hamiltonian (QOCH) is used. The radius from the Eq. (2.1) is expanded up to $\lambda = 3$ and excitations are described by considering quadrupole and octupole collective coordinates. When axial symmetry is imposed, in order to collective coordinates can be parameterized in terms of two deformation parameters β_2 and β_3 and three Euler angles ($\Omega = \phi, \theta, \psi$) [14]. Three Euler angles determine the orientations of the main axes in the laboratory frame [12], while parameters $a_{\lambda,\mu}$ are expressed in terms of deformation parameters β:

$$a_{\lambda\mu} = \beta_\lambda D^\lambda_{0\mu}, \tag{2.46}$$

where $D^\lambda_{\mu\nu}$ is a Wigner function. The classical collective Hamiltonian can be expressed as a sum of the vibrational and rotational kinetic energy and the collective potential. The vibrational kinetic energy can be written as:

$$\mathcal{T}_{\text{vib}} = \frac{1}{2} B_{22} \dot{\beta_2^2} + B_{23} \dot{\beta_2} \dot{\beta_3} + \frac{1}{2} B_{33} \dot{\beta_3^2}, \tag{2.47}$$

where parameters B_{22}, B_{23} and B_{33} are called mass parameters and are functions of deformation parameters β_2 and β_3. The rotational kinetic energy can be written as:

$$\mathcal{T}_{\text{rot}} = \frac{1}{2} \sum_{k=1}^{3} \mathcal{I}_k \omega_k^2, \tag{2.48}$$

where $\mathcal{I}_k$ represents a moment of inertia, which is also a function of deformation parameters. After quantization, the collective Hamiltonian can be written in the

following form:

$$\begin{aligned}\hat{H}_{\text{coll}} = &-\frac{\hbar^2}{2\sqrt{\omega\mathcal{I}}}\left[\frac{\partial}{\partial\beta_2}\sqrt{\frac{\mathcal{I}}{\omega}}B_{33}\frac{\partial}{\partial\beta_2} - \frac{\partial}{\partial\beta_2}\sqrt{\frac{\mathcal{I}}{\omega}}B_{23}\frac{\partial}{\partial\beta_3}\right.\\ &-\frac{\partial}{\partial\beta_3}\sqrt{\frac{\mathcal{I}}{\omega}}B_{23}\frac{\partial}{\partial\beta_2} + \frac{\partial}{\partial\beta_3}\sqrt{\frac{\mathcal{I}}{\omega}}B_{22}\frac{\partial}{\partial\beta_3}\\ &\left.+\frac{\hat{J}^2}{2\mathcal{I}} + V_{\text{coll}}(\beta_2,\beta_3),\right.\end{aligned} \tag{2.49}$$

where $\omega = B_{22}B_{33} - B_{23}^2$ and the corresponding volume element in the collective space is expressed as

$$\int d\tau_{\text{coll}} = \int \sqrt{\omega\mathcal{I}}d\beta_2 d\beta_3 d\Omega. \tag{2.50}$$

To solve the eigenvalue problem of the collective Hamiltonian in Eq. (2.49), eigenfunctions are expanded in terms of a complete set of basis functions. For each value of the angular momentum I, the basis is defined as:

$$|n_2 n_3 IMK\rangle = (\omega\mathcal{I})^{-1/4}\,\phi_{n_2}(\beta_2)\phi_{n_3}(\beta_3)\,|IMK\rangle\,, \tag{2.51}$$

where ϕ_{n_2} and ϕ_{n_3} denote the one-dimensional HO wave functions of β_2 and β_3. For axially deformed shapes, the intrinsic projection of the total angular momentum $K = 0$. The collective wave function can be written as:

$$\Psi_\alpha^{IM\pi}(\beta_2,\beta_3,\Omega) = e^{-\mu^2\beta^2/2}\psi_\alpha^{I\pi}(\beta_2,\beta_3)\,|IM0\rangle\,, \tag{2.52}$$

where the factor $e^{-\mu^2\beta^2/2}$ ensures that the wave functions will vanish at large deformations ($\beta \to \infty$) [32]. The dimensionless parameter μ is called the basis parameter and will be discussed in the third chapter. The probability density distribution is written as:

$$\rho_\alpha^{I\pi}(\beta_2,\beta_3) = e^{-\mu^2\beta^2}\sqrt{\omega\mathcal{I}}\left|\psi_\alpha^{I\pi}(\beta_2,\beta_3)\right|^2, \tag{2.53}$$

with the normalization:

$$\int \rho_\alpha^{I\pi}(\beta_2,\beta_3)d\beta_2 d\beta_3 = 1. \tag{2.54}$$

The reduced transition rates are calculated from the relation:

$$B(E\lambda; I_i \to I_f) = \langle I_i 0\lambda 0|I_f 0\rangle^2 \left|\int d\beta_2 d\beta_3 \sqrt{\omega\mathcal{I}}\psi_i \mathcal{M}_{E\lambda}(\beta_2,\beta_3)\psi_f^*\right|^2, \tag{2.55}$$

where $\mathcal{M}_{E\lambda}(\beta_2, \beta_3)$ is the electric moment of order λ. The electric moment is calculated in microscopic models as $\left\langle \Phi(\beta_2, \beta_3) \left| \hat{\mathcal{M}}_{E\lambda} \right| \Phi(\beta_2, \beta_3) \right\rangle$, with $\Phi(\beta_2, \beta_3)$ representing the nuclear wave function. The corresponding operators for dipole, quadrupole and octupole transitions read:

$$D_1 = \sqrt{\frac{3}{4\pi}} e \left(\frac{N}{A} z_p - \frac{Z}{A} z_n \right), \tag{2.56}$$

$$Q_2^p = \sqrt{\frac{5}{16\pi}} e (2z_p^2 - x_p^2 - y_p^2), \tag{2.57}$$

$$Q_3^p = \sqrt{\frac{7}{16\pi}} e \left[2z_p^3 - 3z_p(x_p^2 + y_p^2) \right]. \tag{2.58}$$

There are five parameters from Eq. (2.49) that need to be determined. These are the three mass parameters B_{22}, B_{23} and B_{33}, the collective potential V_{coll} and the moment of inertia $\mathcal{I}$. They are determined by constrained SCMF calculations for the chosen DD-PC1 functional and the chosen pairing interaction. Deformation parameters are determined from following relations:

$$\beta_2 = \frac{\sqrt{5\pi}}{3AR_0^2} \left\langle \hat{Q}_2 \right\rangle, \tag{2.59}$$

$$\beta_3 = \frac{\sqrt{7\pi}}{3AR_0^3} \left\langle \hat{Q}_3 \right\rangle, \tag{2.60}$$

where $R_0 = r_0 A^{1/3}$ and $r_0 = 1.2$fm. Moments of inertia are calculated according to the Inglis-Belyaev formula [13]:

$$\mathcal{I} = \sum_{i,j} \frac{(u_i v_j - v_i u_j)}{E_i + E_j} \left| \left\langle i \left| \hat{\mathbf{J}} \right| j \right\rangle \right|^2, \tag{2.61}$$

where $\hat{\mathbf{J}}$ is the angular momentum along the axis perpendicular to the symmetric axis, u_i and v_i are occupation probabilities and E_i are quasiparticle energies. The summation runs over the proton and neutron quasiparticle states. The single-nucleon wave functions ψ_i are determined from the solutions of the constrained RMF+BCS equations. Mass parameters are calculated by using the perturbative cranking ap-

proximation:

$$B_{\lambda\lambda'}(q_2,q_3)=\frac{\hbar^2}{2}\left[\mathcal{M}_{(1)}^{-1}\mathcal{M}_{(3)}\mathcal{M}_{(1)}^{-1}\right]_{\lambda\lambda'}, \tag{2.62}$$

with

$$\mathcal{M}_{(n),\lambda\lambda'}(q_2,q_3)=\sum_{i,j}\frac{\left\langle i\left|\hat{Q}_\lambda\right|j\right\rangle\left\langle j\left|\hat{Q}_{\lambda'}\right|i\right\rangle}{(E_i+E_j)^n}(u_iv_j+v_iu_j)^2. \tag{2.63}$$

The potential energy surface (PES) includes the energy of zero-point motion that needs to be subtracted. The vibrational and rotational zero-point energies (ZPE) are subtracted by calculating corrections on these energies using the cranking approximation:

$$\Delta V_{\text{vib}}(\beta_2,\beta_3)=\frac{1}{4}\text{Tr}\left[\mathcal{M}_{(3)}^{-1}\mathcal{M}_{(2)}\right], \tag{2.64}$$

$$\Delta V_{\text{rot}}(\beta_2,\beta_3)=\frac{\left\langle\hat{\mathbf{J}}^2\right\rangle}{2\mathcal{I}}. \tag{2.65}$$

Subtracting the ZPE corrections from the total mean-field energy, gives the potential V_{coll}:

$$V_{\text{coll}}(\beta_2,\beta_3)=E_{\text{tot}}(\beta_2,\beta_3)-\Delta V_{\text{vib}}(\beta_2,\beta_3)-\Delta V_{\text{rot}}(\beta_2,\beta_3). \tag{2.66}$$

Combined with the RMF model based on a DD-PC1 functional, the QOCH model is used to calculate the low-lying excitation spectra and transition rates. Together, these two methods enable a complete theoretical calculation of the nuclear shapes, collective excitations and transition strengths of transitions between excited states and the ground-state.

3 Results

The calculation was performed using two codes, the DIRHB code [33], which calculates deformation parameters and the PES in the ground-state of a nucleus, and the QOCH code, which was used to calculate excitation energies and transition rates up to $J = 7^-$. In order to plot the PES, energies were calculated for all combinations of deformation parameters $-0.8 \leq \beta_2 \leq 0.8$, $-0.8 \leq \beta_3 \leq 0.8$, with a step of 0.05. This means there are 1089 combinations of deformation parameters and that energies should be calculated at each of these 1089 configurations. Before the calculations are performed, the number of oscillator shells for nucleons, denoted by n0f, needs to be set. For most nuclei, calculations can be performed with n0f=10. For heavier nuclei, calculations had to be performed with n0f=12, because the number n0f=10 was not large enough for RHB calculations to converge. Raising the number of oscillator shells leads to more precise results, but the calculations become extremely time-consuming and the results do not strikingly differ between the calculations with n0f=10 and n0f=12. The calculations were performed on the even-even isotopes of krypton (Kr) ($Z = 36,\ 30 \leq N \leq 66$), xenon (Xe) ($Z = 54,\ 54 \leq N \leq 118$) and barium (Ba) ($Z = 56,\ 54 \leq N \leq 96$). All of these nuclei have a ground-state $J = 0^+$. Quadrupole deformations in the ground-state are very common and were expected to be observed in many of the examined isotopes. Octupole deformations are much rarer, and are expected only for certain nucleon numbers, as was explained. For this reason, it was expected that more octupole deformations in the ground-state would be found among the isotopes of Ba, because the proton number of these isotopes is $Z = 56$. In the first part of this chapter, deformations in the ground-state were examined. Contour plots of the PESs are shown for nuclei with octupole deformations in the ground-state. Also, β_2 and β_3 deformations in the ground-state are plotted as a function of the neutron number N. In the second subchapter, binding energies and deformation energies are plotted as a function of the nucleon number A. Deformation energies E_{def} are defined as $E_{def} = E_{min} - E_{sph}$, where E_{min} is the energy of the global minimum and E_{sph} is the energy of a spherical nucleus ($\beta_2 = \beta_3 = 0$). In the third and fourth subchapter, results for the excitation energies and transition strengths are presented. Calculated binding energies, excitation energies and transition strengths were compared to the experimental data [26].

3.1 Quadrupole and octupole deformations in Kr, Xe and Ba

Qaudrupole deformations were observed in many nuclei. An example is given of an isotope ^{146}Xe in Fig. 3.1. The PES shows an existence of a quadrupole deformation in the ground-state of a given isotope. No octupole deformation is present. Energies shown in the colorbar are given in MeV, which is also true for other figures. Another example of a quadrupole-deformed nuclei is ^{74}Kr (Fig. 3.2), while ^{78}Kr (Fig. 3.3) is an example of a nucleus that is spherical in the ground-state.

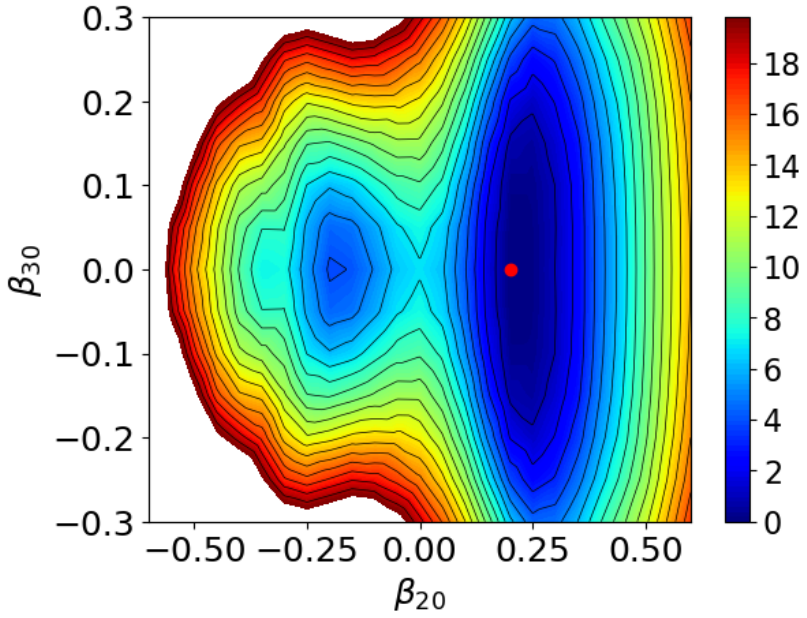

Figure 3.1: The PES of ^{146}Xe. The global minimum (red dot) is at $\beta_2 = 0.2$, $\beta_3 = 0.0$.

Octupole deformations in the ground-state were observed in ^{76}Kr (Fig. 3.4), ^{142}Xe (Fig. 3.5) and in 7 Ba isotopes. In Fig 3.6, the PES for ^{144}Ba is presented. Octupole deformations were also calculated for Ba isotopes ^{112}Ba (Fig. 3.7) and ^{114}Ba (Fig. 3.8). The data on all isotopes for which $\beta_3 \neq 0$ in the ground-state is given in Table 3.1.

The fact that more octupole deformations were observed in Ba isotopes than Kr and Xe isotopes is in agreement with what is empirically suggested [3]. A symmetry of octupole deformation parameters was assumed in the calculations, which is why the same energy was calculated for both (β_2, β_3) and (β_2, $-\beta_3$). It was also observed that at least one Kr and at least one Xe isotopes are octupole-deformed in the ground-state. The fact that in other nuclei $\beta_3 = 0$ in the ground-state, does not mean that these nuclei are not octupole vibrational and that there is no effect of oc-

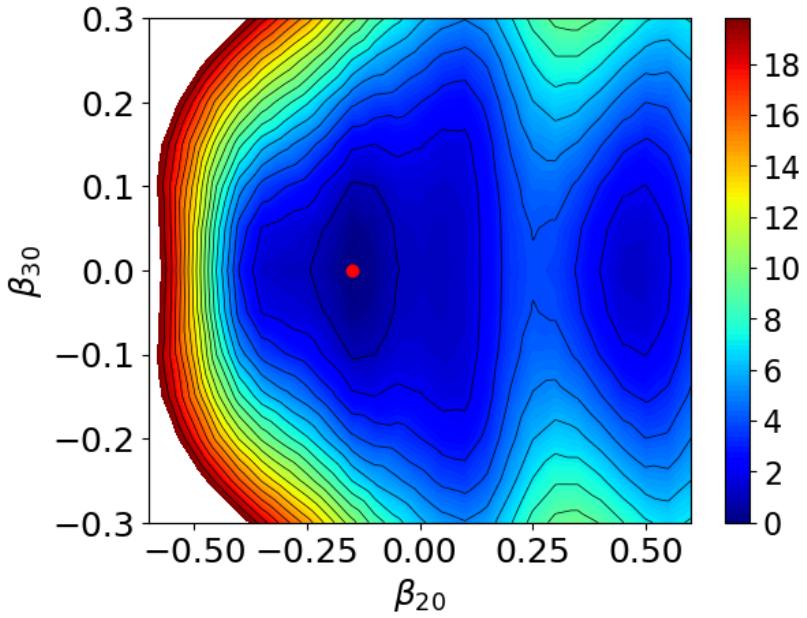

Figure 3.2: ^{74}Kr, $Z = 36, N = 38$. $\beta_2 = -0.15$, $\beta_3 = 0.0$

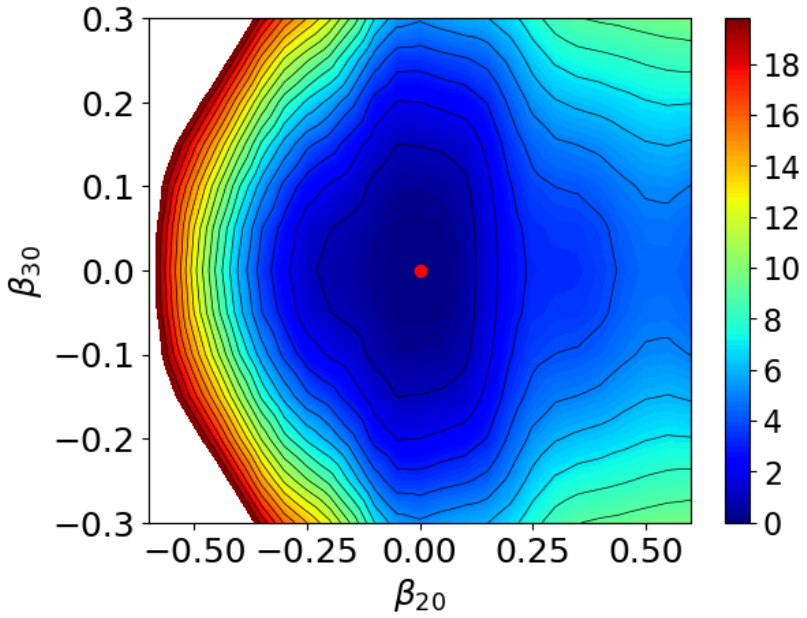

Figure 3.3: ^{78}Kr, $Z = 36, N = 42$. $\beta_2 = 0.0$, $\beta_3 = 0.0$

tupole correlation on the vibrational and rotational spectra [3]. It can be shown that if the nuclear potential becomes very soft with respect to the octupole deformation, the equilibrium deformation becomes a measure of frequency, mass and inertia parameters and not of the deformation parameter [34]. ^{138,140}Xe and ^{140,142}Ba isotopes, for example, are β_2 and β_3 soft and become reflection asymmetric at medium spins. ^{146}Xe was calculated to have a well-developed quadrupole ground-state deformation, but is β_3 soft [3]. At low rotational frequencies, negative-parity states of this nucleus

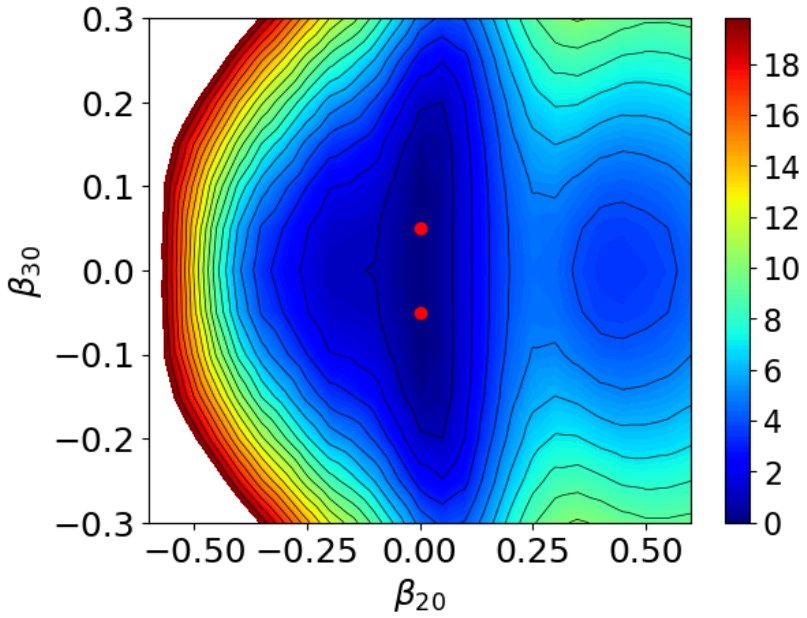

Figure 3.4: ^{76}Kr, $Z = 36, N = 40$. $\beta_2 = 0.0$, $\beta_3 = \pm 0.05$

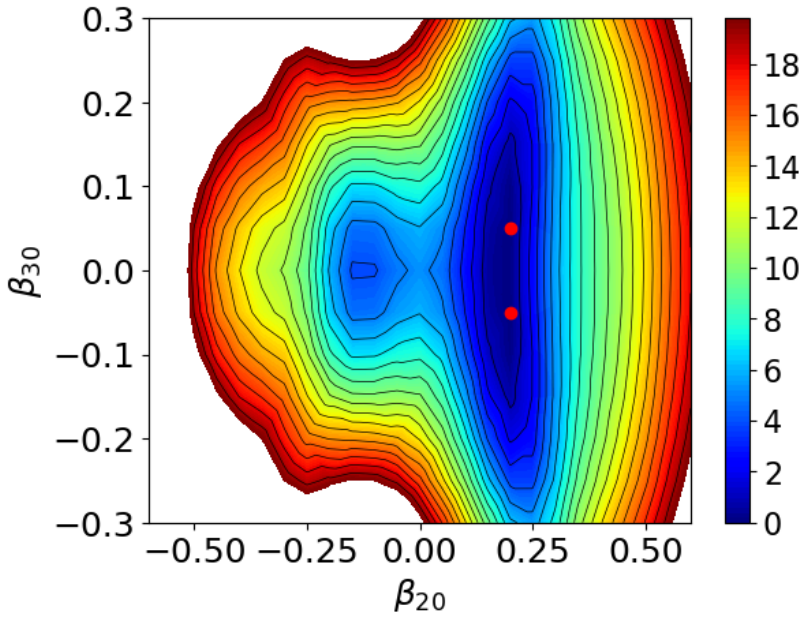

Figure 3.5: ^{142}Xe, $Z = 54, N = 88$. $\beta_2 = 0.2$, $\beta_3 = \pm 0.05$

can be described in terms of very collective octupole deformations.

The values of both β_2 and β_3 in the ground-state were plotted as functions of the neutron number for Kr, Xe and Ba isotopes, as is shown in Fig. 3.9. The red line with red dots represents the calculated values of β_2, while the green line with green dots represents the calculated values of β_3. The black line represents a $\beta = 0$ position and it is plotted so that isotopes with zero quadrupole $\beta_2 = 0$ or octupole $\beta_3 = 0$ deformation in the ground-state can be seen. As was already shown in Table 3.1, and

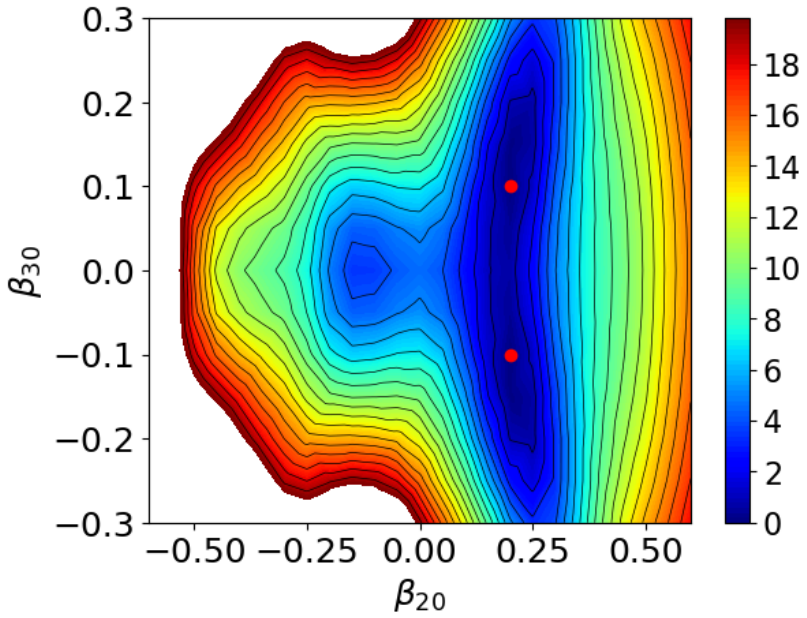

Figure 3.6: ^{144}Ba, $Z = 56, N = 88$. $\beta_2 = 0.2$, $\beta_3 = \pm 0.1$

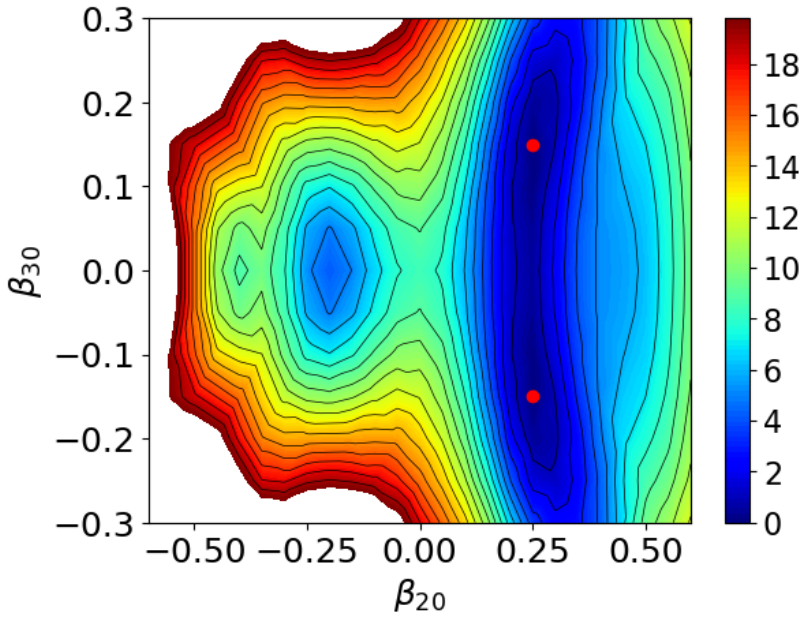

Figure 3.7: ^{112}Ba, $Z = 56, N = 56$. $\beta_2 = 0.25$, $\beta_3 = \pm 0.15$

can be seen in Fig. 3.9, octupole deformations can be found in one Kr isotope, one Xe isotope and 7 Ba isotopes. The Kr isotope with the biggest quadrupole deformation is ^{72}Kr with $\beta_2 = -0.35$. Two Kr isotopes are spherical in the ground-state, ^{78}Kr and ^{86}Kr. The most quadrupole-deformed Xe isotope is ^{154}Xe with $\beta_2 = 0.35$ and only one Xe isotope, ^{136}Xe, is spherical in the ground-state. Most octupole-deformed isotopes were found in Ba isotopes, which confirms the empirical knowledge. Also, the existence of octupole-deformed nuclei was calculated for regions ($Z \approx 34$, $N \approx 34$)

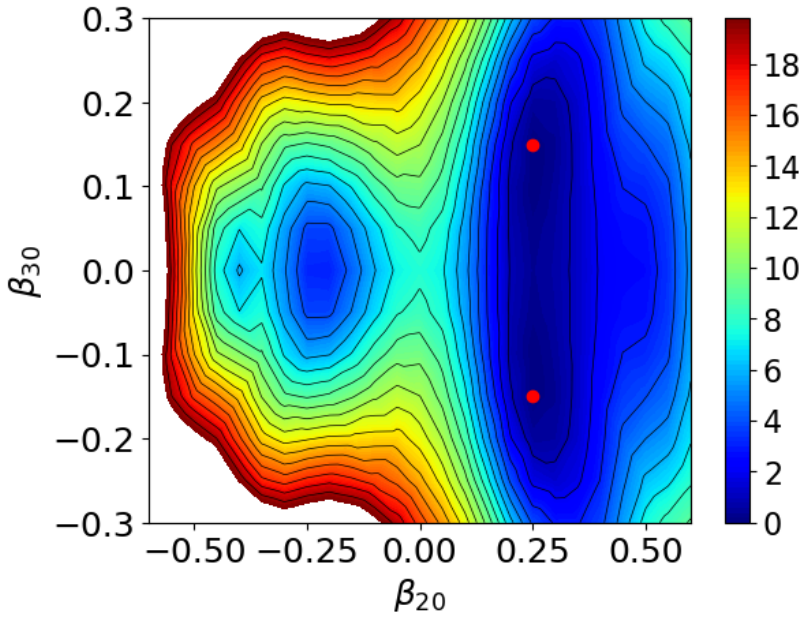

Figure 3.8: ^{114}Ba, $Z = 56, N = 58$. $\beta_2 = 0.25$, $\beta_3 = \pm 0.15$

Isotope	Z	N	β_2	β_3
^{76}Kr	36	40	0.0	$\pm$ 0.05
^{142}Xe	54	88	0.2	$\pm$ 0.05
^{112}Ba	56	56	0.25	$\pm$ 0.15
^{114}Ba	56	58	0.25	$\pm$ 0.15
^{144}Ba	56	88	0.2	$\pm$ 0.1
^{146}Ba	56	90	0.25	$\pm$ 0.15
^{148}Ba	56	92	0.25	$\pm$ 0.15
^{150}Ba	56	94	0.3	$\pm$ 0.15
^{152}Ba	56	96	0.3	$\pm$ 0.05

Table 3.1: Deformation parameters of the nuclei with observed octupole deformations in the ground-state

(^{76}Kr) and ($Z \approx 56,\ N \approx 56$) (^{112,114}Ba). The Ba isotope with the biggest quadrupole deformation is ^{116}Ba, with $\beta_2 = 0.4$, which makes this isotope the most quadrupole-deformed isotope out of all the examined isotopes. The only Ba isotope that is spherical in the ground-state is ^{138}Ba. What can be observed is that isotopes with $N = 50, 82$ are spherical in the ground state. These N are magic numbers [1]. For these numbers, neutron shells are completely filled and, as a result, these nuclei are more stable than other nuclei. Isotopes with N in the vicinity of the magic number have lower values of deformation parameters and are sometimes spherical, as is the case with ^{78}Kr. From Fig. 3.9 it can be seen that quadrupole deformation parameter increases as N becomes more distant from the magic number and decreases as it gets closer to

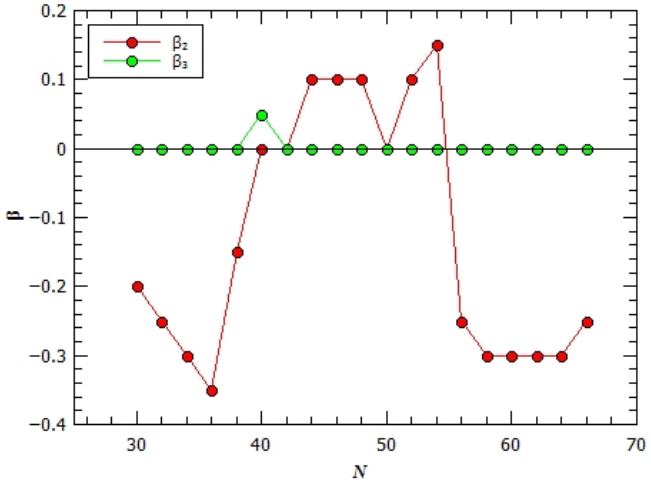

(a) Kr

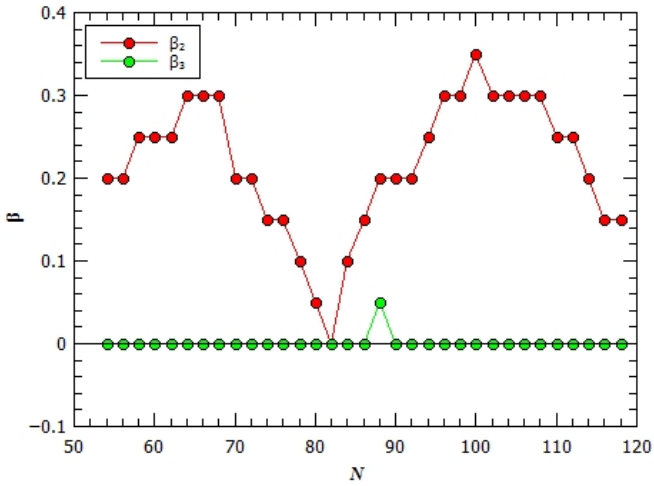

(b) Xe

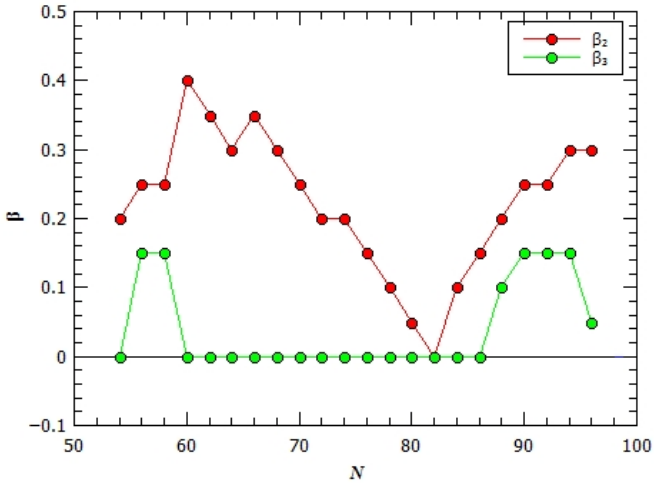

(c) Ba

Figure 3.9: Parameters of deformation β_2 and β_3 in the ground-state as functions of the neutron number for isotopes of Kr, Xe and Ba. The black line indicates $\beta = 0$.

the next magic number. The next known magic number after 82 is 126, which is why β_2 starts decreasing for Xe isotopes above ^{154}Xe ($N = 100$).

3.2 Binding energies and deformation energies

Binding energies E_B were calculated and compared with the available experimental data [26]. It should be noted that even-even Kr isotopes with $N < 34$ and $N > 64$, Xe isotopes with $N > 94$ and Ba isotopes with $N < 56$ have not been experimentally observed yet [26], so there is no available experimental data for these isotopes. In Fig. 3.10, binding energy per nucleon number A is plotted as a function of A for Kr, Xe and Ba isotopes. Red line with red dots represents the calculated values of E_B/A, while the unconnected dots with the red edge represent the experimentally observed values of E_B/A. Error bars are not shown on these graphs because they are too small to be visible on such a large scale. What can be seen from Fig. 3.10 is that the calculated values of E_B/A are in an extremely good agreement with the experimentally measured values.

Deformation energies E_{def} represent the energy difference between energies in the global minimum of a nucleus E_{min}, and energies of the spherical nuclear shape E_{sph}. These energies are also plotted as a function of A in Fig. 3.11. Similarly to Fig. 3.10, red lines with red dots represent the calculated E_{def} values, while the black line represents a $E_{def} = 0$ position, which corresponds to a spherical nucleus. As expected, $E_{def} = 0$ for nuclei with magic neutron number, since it was already calculated that these nuclei are spherical in the ground-state. There are two spherical nuclei among Kr isotopes and one spherical nucleus among Xe and Ba isotopes. Nuclei with neutron numbers next to the magic number have a very low deformation energy. For ^{76}Kr ($N = 40$), a subshell closure occurs. For this nuclei, the last two neutrons occupy the $p_{1/2}$ subshell, making it completely filled. This can be seen in Fig. 2.1. For this reason, ^{76}Kr has $\beta_2 = 0$ in the ground-state and has a low octupole deformation $\beta_3 = \pm 0.05$. For this reason, the deformation energy of this nuclei is very low, $E_{def} = 0.003685$ MeV. Next to ^{76}Kr isotope is ^{78}Kr isotope, which also has $\beta_2 = 0$ and is not octupole-deformed, so $E_{def} = 0$. As is the case with β_2 parameters, higher values of E_{def} are found among isotopes that are at a larger distance from isotopes with magic neutron number on a graph. The Kr isotope with the largest E_{def} is ^{96}Kr.

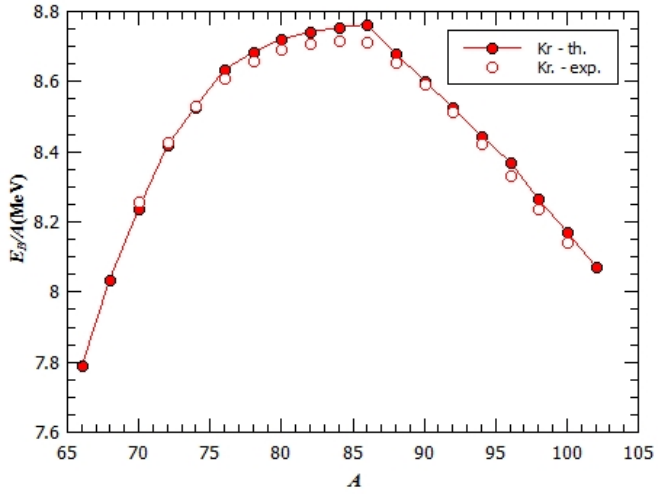

(a) Kr

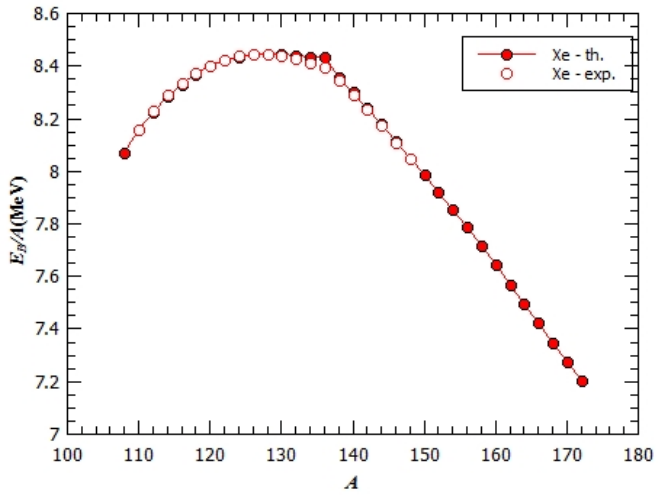

(b) Xe

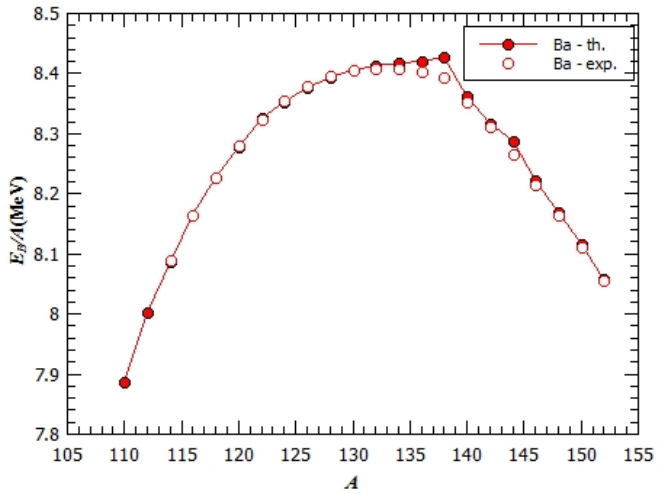

(c) Ba

Figure 3.10: Binding energy per nucleon number E_B/A as a function of the nucleon number A for Kr, Xe and Ba isotopes.

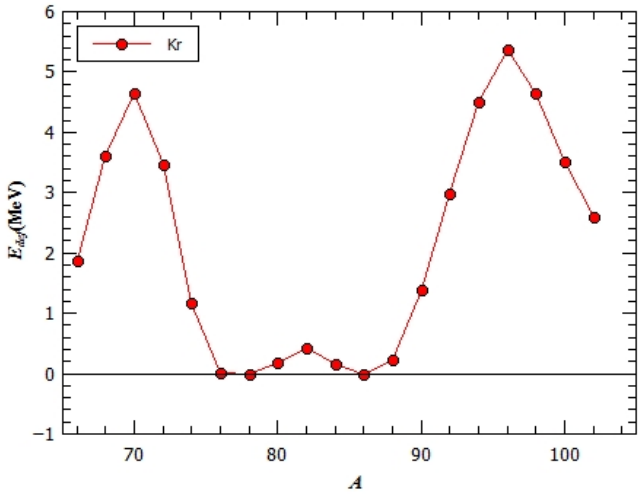

(a) Kr

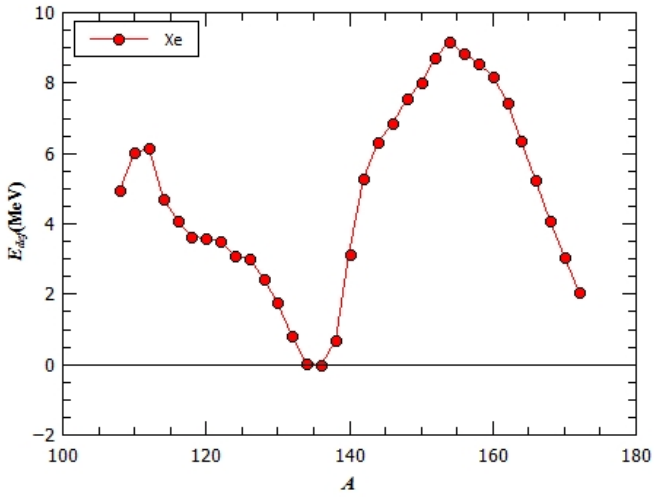

(b) Xe

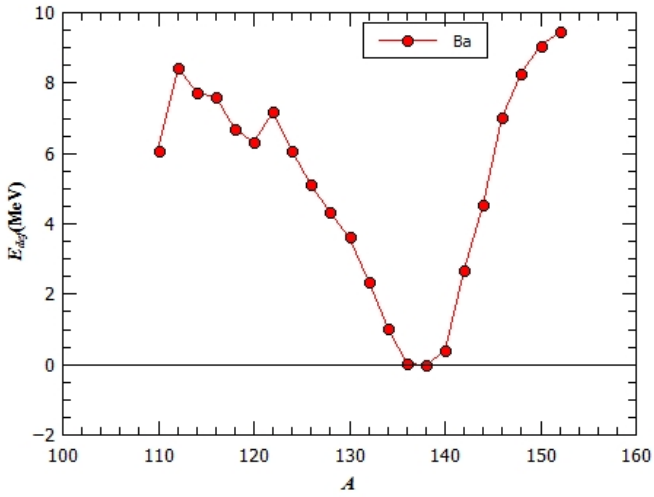

(c) Ba

Figure 3.11: Deformation energy E_{def} as a function of the nucleon number A for Kr, Xe and Ba isotopes. The black line indicates $E_{def} = 0$.

For Xe and Ba isotopes, the largest E_{def} values were calculated for ^{154}Xe and ^{152}Ba.

For another type of deformation energy, we define octupole deformation energy, $E_{oct} = E_{min}(\beta_2, \beta_3) - E_{quad}(\beta_2, \beta_3 = 0)$, where $E_{min}(\beta_2, \beta_3)$ is the energy of the global minimum and $E_{quad}(\beta_2, \beta_3 = 0)$ is the energy of the state that has the same quadrupole deformation as the global minimum, but no octupole deformation. From this definition, it follows that $E_{oct} \neq 0$ only for those isotopes that show an octupole deformation in the ground-state. For ^{76}Kr, $E_{oct} = 0.003685$ MeV, and for ^{142}Xe, $E_{oct} = 0.031573$ MeV. Both of these energies have very small values and the reason for that is the low value of $\beta_3 = \pm 0.05$. For Ba isotopes, E_{oct} was plotted as a function of A, which can be seen in Fig. 3.12. The Ba isotope with the smallest value

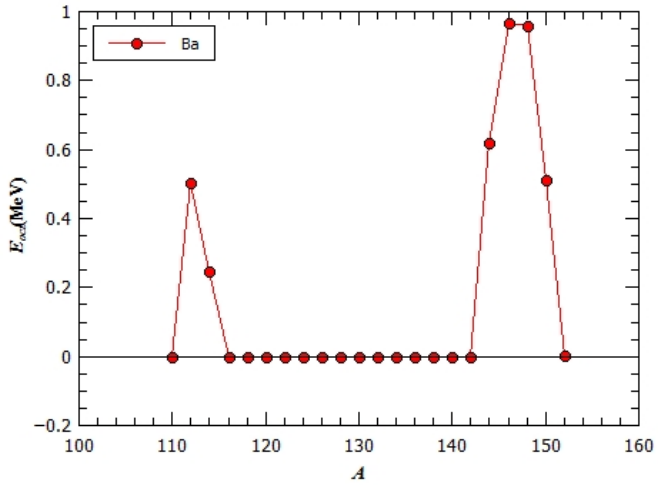

Figure 3.12: The octupole deformation energy E_{oct} as a function of the nucleon number A for Ba isotopes. The black line indicates $E_{oct} = 0$

of E_{oct} is ^{152}Ba with $E_{oct} = 0.001307$ MeV and $\beta_3 = \pm 0.05$, while the largest value $E_{oct} = 0.967133$ MeV is found in ^{146}Ba ($\beta_3 = \pm 0.15$). The general rule, with some exceptions, is that E_{oct} becomes higher for nuclei with larger β_3 in the ground-state.

3.3 Setting the basis parameter

Before the QOCH code is used to calculate low-lying excitation spectra and transition strengths, the basis parameter μ from equations (2.52) and (2.53) needs to be set. The condition for setting the value of μ is that the ground-state energy and excitation energies need to remain constant with respect to the value of μ. From this condition, a range of μ values, for which the ground-state energy and excitation energies remain

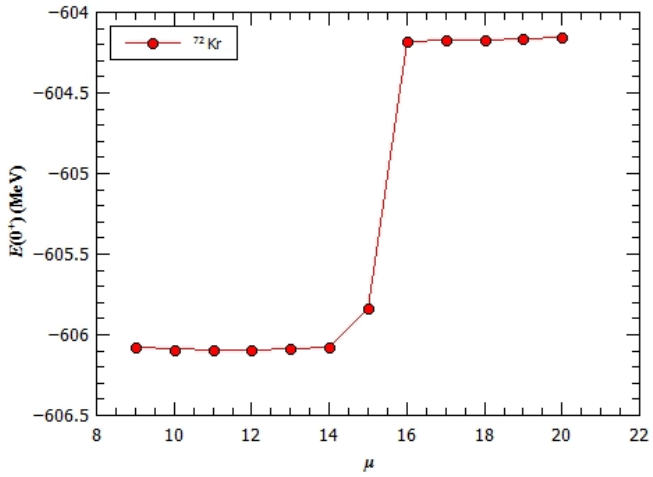

(a) ^{72}Kr

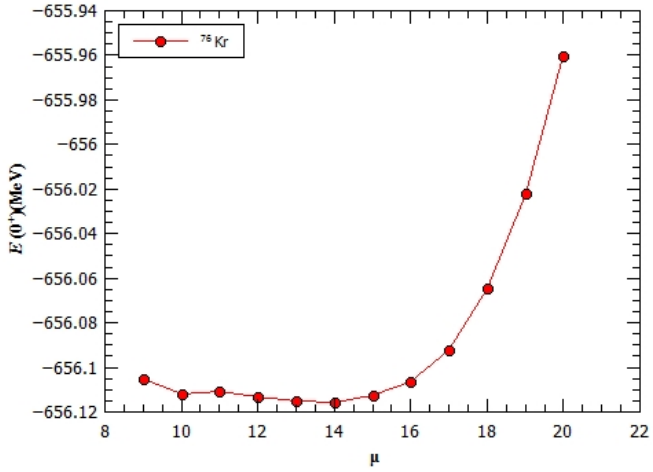

(b) ^{76}Kr

Figure 3.13: Ground-state energy $E(0^+)$ as a function of the basis parameter μ for isotopes ^{72}Kr and ^{76}Kr.

constant, can be determined. From this range, a value of μ can be taken and set for future calculations. In order to determine this range, the ground-state energy and excitation energies of ^{72}Kr and ^{76}Kr were plotted as a function of μ. The basis parameter μ was varied from $\mu = 9$ to $\mu = 20$ with a step of 1. Fig. 3.13 shows the calculated ground-state energy of ^{72}Kr and ^{76}Kr plotted as a function of μ. It can be seen that for both isotopes, the ground-state energy is stable in the interval $9 \leq \mu \leq 14$. For $\mu > 14$, the ground-state energy of ^{72}Kr rises approximately 2 MeV. For ^{76}Kr, the ground-state energy rises for $\mu > 15$, but the rise is much lower than the rise in ^{72}Kr. For $\mu = 20$, $E(0^+)$ is less than 0.2 MeV higher than $E(0^+)$ for $\mu = 9$.

For both ^{72}Kr and ^{76}Kr, excitation energies of the first 2^+, 4^+ and 6^+ positive-

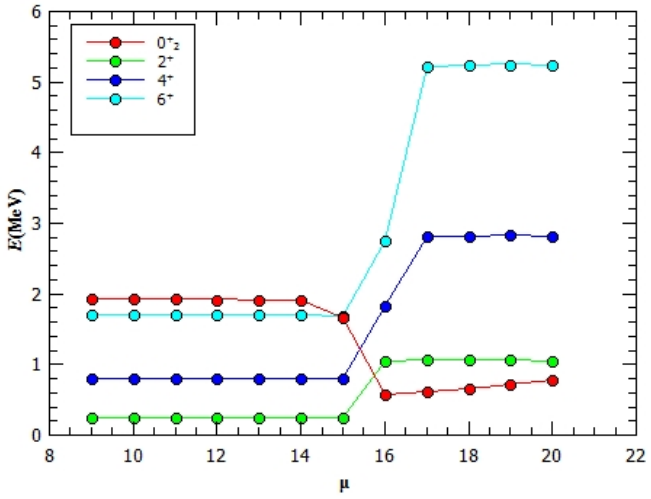

(a) ^{72}Kr

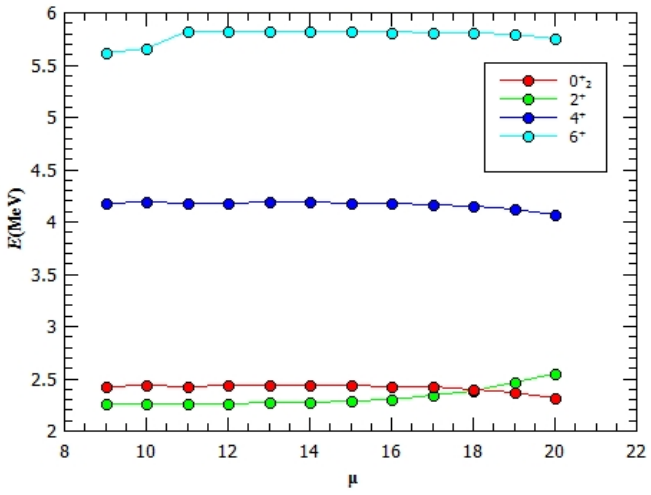

(b) ^{76}Kr

Figure 3.14: Excitation energies of 2^+, 4^+,6^+ and 0_2^+ states as functions of the basis parameter μ for isotopes ^{72}Kr and ^{76}Kr.

parity states and the second 0^+ positive-parity state (0_2^+) were plotted as a function of μ in Fig. 3.14. For ^{72}Kr, excitation energies of all states are stable in the interval $9 \leq \mu \leq 15$, except for 0_2^+, which is stable for $9 \leq \mu \leq 14$. The situation is different for ^{76}Kr. The excitation energy of 2^+ and 0_2^+ states remain constant in the interval $9 \leq \mu \leq 14$. The excitation energy of the 4^+ state is stable for all values of μ that were taken into consideration , while the excitation energy of the 6^+ state remains stable for $\mu > 10$.

Excitation energies of the first 1^-, 3^-, 5^- and 7^- negative-parity states were also plotted as a function of μ for isotopes ^{72}Kr and ^{76}Kr. The results are shown in Fig.

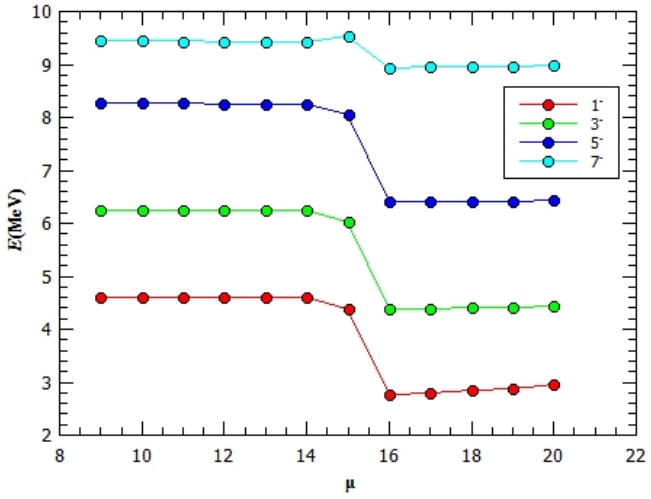

(a) ^{72}Kr

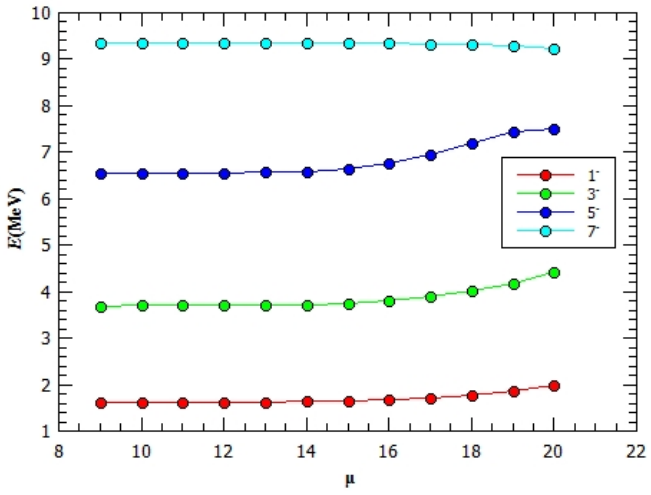

(b) ^{76}Kr

Figure 3.15: Excitation energies of 1^-, 3^-,5^- and 7^- states as functions of the basis parameter μ for isotopes ^{72}Kr and ^{76}Kr.

3.15. For ^{72}Kr, all excitation energies remain constant in the interval $9 \leq \mu \leq 14$. For ^{76}Kr, energies of states 1^- and 7^- remain a constant for $\mu < 18$ and the change is relatively small outside this interval. Excitation energies of 3^- and 5^- states are stable for $\mu < 16$ and the change outside the interval is larger than the change for two other states. If all results are taken into account, the interval in which all calculated energies remain stable is $11 \leq \mu \leq 14$. According to another calculation [32], energies remain stable in the interval $8 \leq \mu \leq 15$. The basis parameter was set to $\mu = 13$, because this value belongs to both of the calculated intervals.

3.4 Low-lying excitation energy spectra

Excitation energies of the low-lying states were calculated for positive-parity states 2^+, 4^+, 6^+ and 0_2^+, and for negative-parity states 1^-, 3^-, 5^- and 7^-. Calculated energies were plotted as a function of N for isotopes of Kr, Xe and Ba. Both the positive- and negative-parity states were plotted in the following figures, each showing the results for two states. All results were compared with the available experimental data [26], which is represented with unconnected dots on a graph. The scale of graphs was too large for error bars to be visible, so experimental results are shown without error bars. Results for positive-parity states 0_2^+, 2^+ and 4^+, 6^+ are shown in figures 3.16 and 3.17.

Calculated excitation energies of the first 2^+, 4^+ and 6^+ states are in good agreement with experimental values of those energies for Xe and Ba isotopes, with the exception for isotopes with N near or equal to the magic number 82. This was expected because for magic numbers, single-particle excitations contribute more to low-lying excitation spectra than collective excitations. The results for 0_2^+ state for all isotopes do not show a good agreement with experimental results, with the exception of some isotopes. This shows that, in general, the QOCH code, as was used in this work, does not give good results for 0_2^+ state. For Kr, calculated excitation energies of 2^+, 4^+ and 6^+ states show a good agreement with the results mostly for heavier nuclei with $N \geq 56$ and for ^{72}Kr. Most of the calculated excitation energies for Kr isotopes have higher values than the experimental ones. This was expected for nuclei around ^{76}Kr due to the neutron subshell closure $N = 40$ and around ^{86}Kr, because $N = 50$ is a magic number. Isotopes between ^{76}Kr and ^{86}Kr are characterised by either $\beta_2 = 0$ or by lower values of β_2, as can be seen from Fig. 3.9. The positive-parity states are mostly accounted for by the quadrupole correlations. If the nucleus is not sufficiently quadrupole deformed in the SCMF calculations, it is expected that the QOCH model also does not give a very good result for positive-parity excited states. Highest quadrupole deformations in Kr isotopes occur for $N = 36$ and $N \geq 56$, which is why for those isotopes there is good agreement between theory and experiment. Ba and Xe isotopes, on the other hand, are characterised by larger β_2 values and the potentials are more rigid in β_2, with the exception of isotopes with N near or equal to 82. For this reason, the QOCH method gives better results for Xe and Ba isotopes. Also, another reason why the QOCH method might not give good results

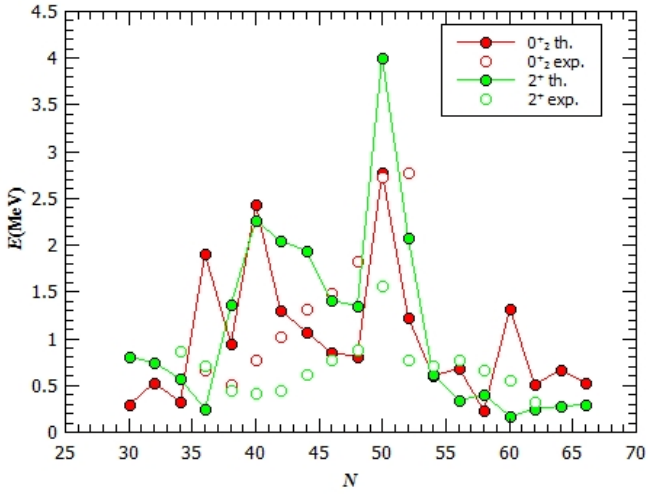

(a) Kr

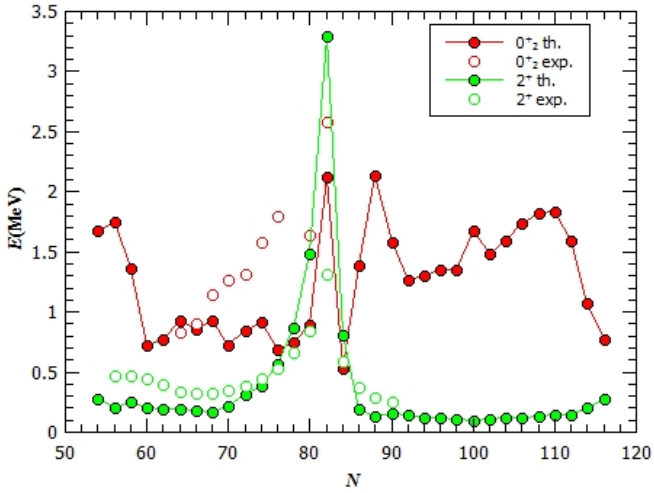

(b) Xe

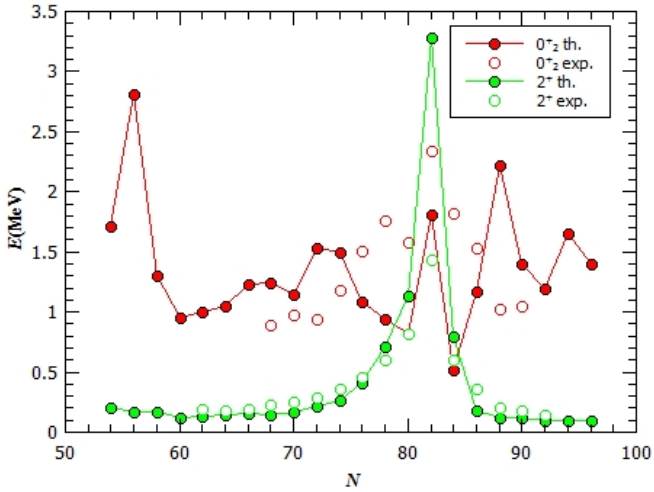

(c) Ba

Figure 3.16: Excitation energies E of states 0_2^+ and 2^+ as functions of the neutron number N for Kr, Xe and Ba isotopes.

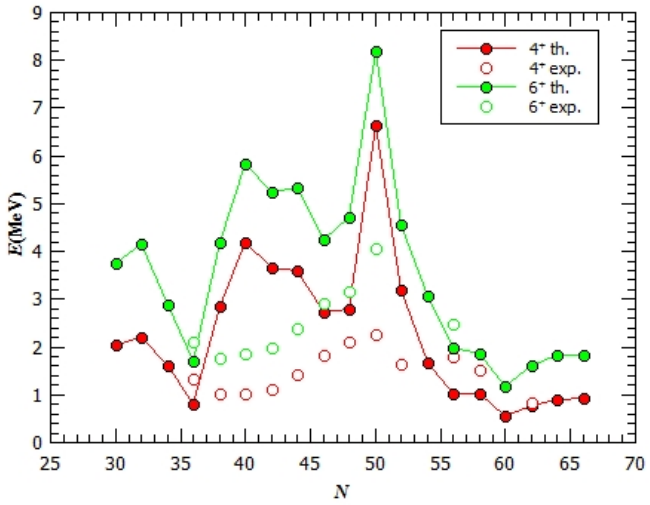

(a) Kr

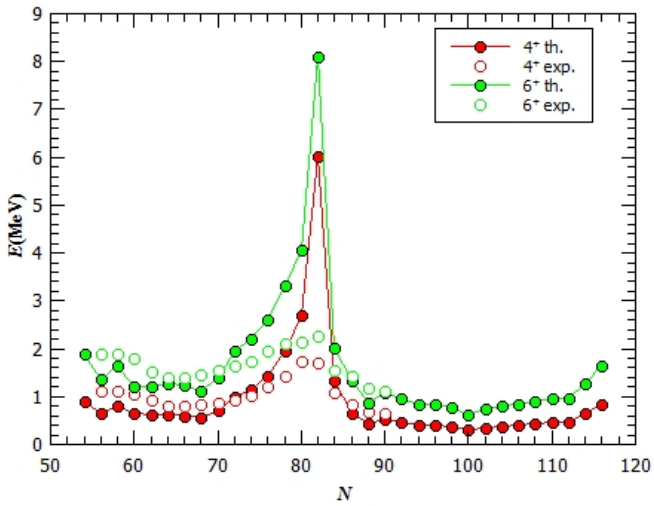

(b) Xe

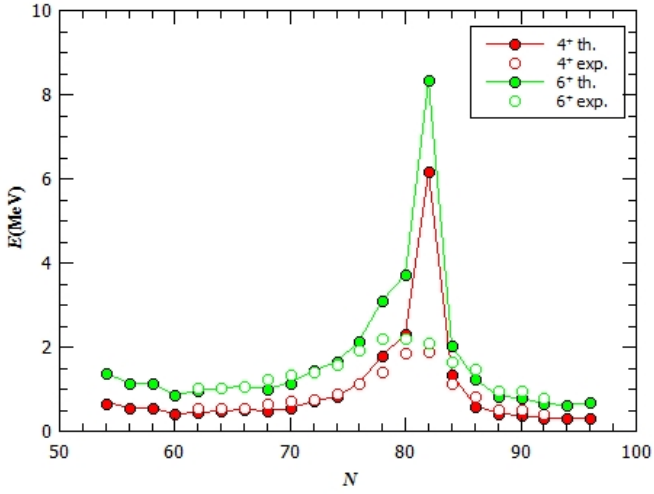

(c) Ba

Figure 3.17: Excitation energies E of states 4^+ and 6^+ as functions of the neutron number N for Kr, Xe and Ba isotopes.

for Kr isotopes is because in all of the calculations axial symmetry is assumed and the triaxial deformation parameter γ is ignored [32]. If the potential energy surfaces for these Kr nuclei are soft in γ deformation, the triaxial degree of freedom is considered a non-negligible effect and the axially-symmetric QOCH approach may not be good enough.

Results for negative-parity states are shown in figures 3.18 and 3.19. Experimental results for energies of 1^- state are rarer than the results for other states, there are only two results for Kr, one for Xe and seven for Ba isotopes. For the same N, calculated energies are always higher for states with higher angular momentum. That is not always the case for experimental results. For example, the 1^- state is often higher than the 3^- state. This means that for some nuclei, a low-lying excitation spectra cannot be completely accounted for by the collective model. It can be observed that the results for negative-parity states, with the exception of the 1^- state, are mostly not in a good agreement with experimental results, with the calculated values of excitation energies being much higher than experimental values. The results are in good agreement with experimental data for the heaviest Xe and Ba isotopes, with $N \geq 86$. For Kr isotopes there is a large difference between calculated and experimental results, by more than 2 MeV for many nuclei. While quadrupole correlations are responsible for the existence of low-lying positive-parity states, octupole correlations are responsible for the existence of low-lying negative-parity states. As can be seen in Fig. 3.9, the only Kr isotope with $\beta_3 \neq 0$ is ^{76}Kr, which has a low octupole deformation parameter value $\beta_3 = \pm 0.05$. Because of this, calculated excitation energies are not in good agreement with experimental values. While it is true that octupole deformation in the ground-state was only found in one Xe isotope, ^{142}Xe, some of the Xe isotopes are β_3-soft in the ground-state, so the QOCH method gives good results. This explains why the results are in good agreement with experimental data for Xe isotopes with $N \geq 86$. Most octupole deformations in the ground-state were observed among Ba isotopes. All $N \geq 86$ Ba isotopes were found to be octupole-deformed in the ground-state. Some of the Ba isotopes are also β_3-soft in the ground-state. For this reason, the QOCH method gives good results for the heaviest examined Ba isotopes. These results could also be improved by including the triaxial degree of freedom γ. This would improve the results for nuclei that are γ-soft in the ground-state.

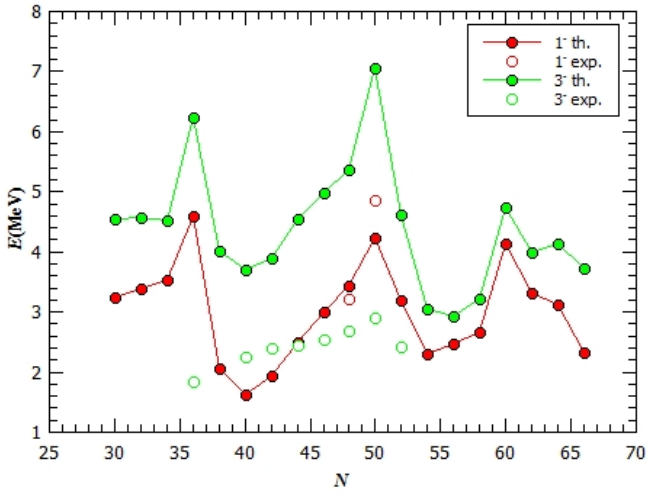

(a) Kr

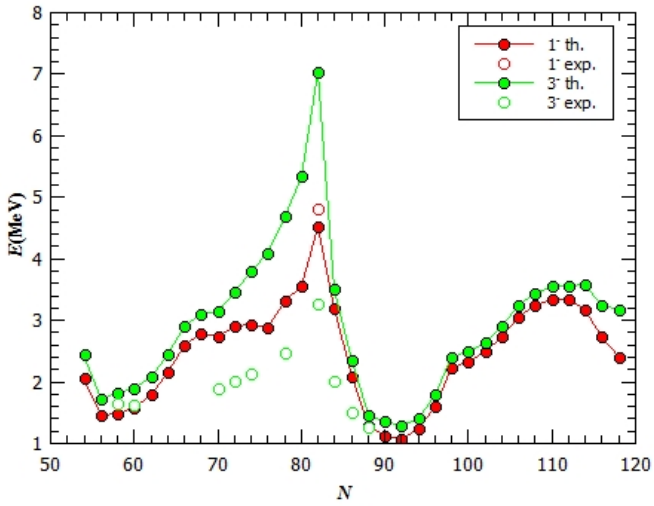

(b) Xe

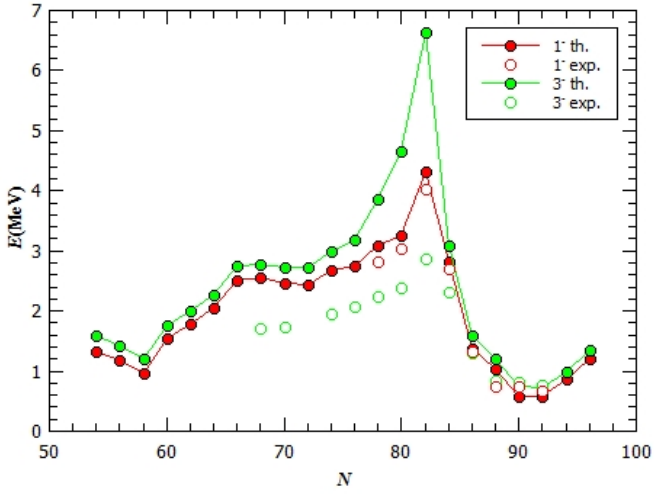

(c) Ba

Figure 3.18: Excitation energies E of states 1^- and 3^- as functions of the neutron number N for Kr, Xe and Ba isotopes.

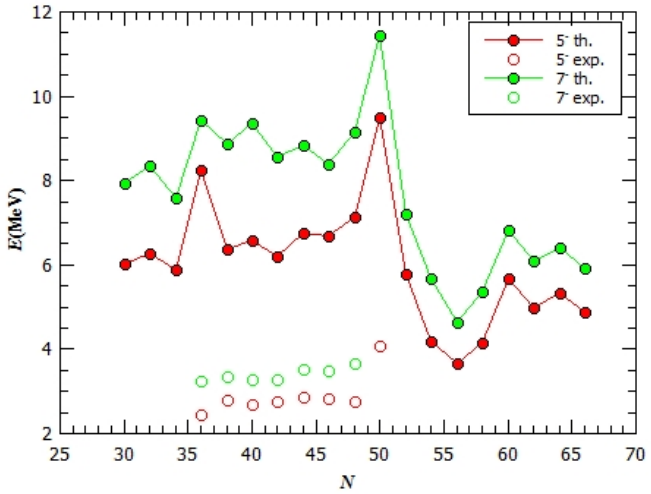

(a) Kr

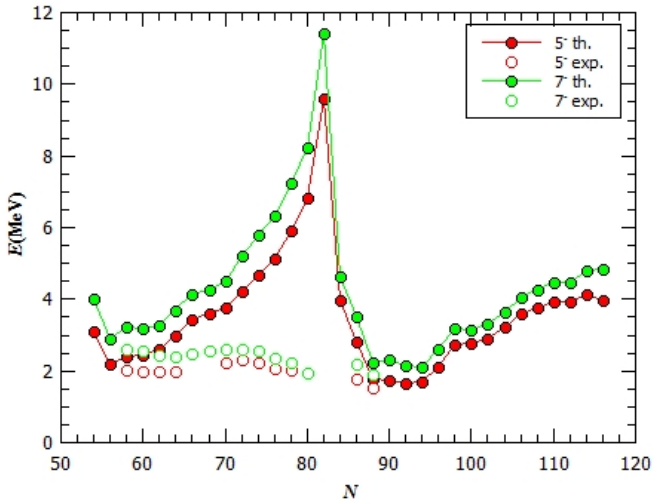

(b) Xe

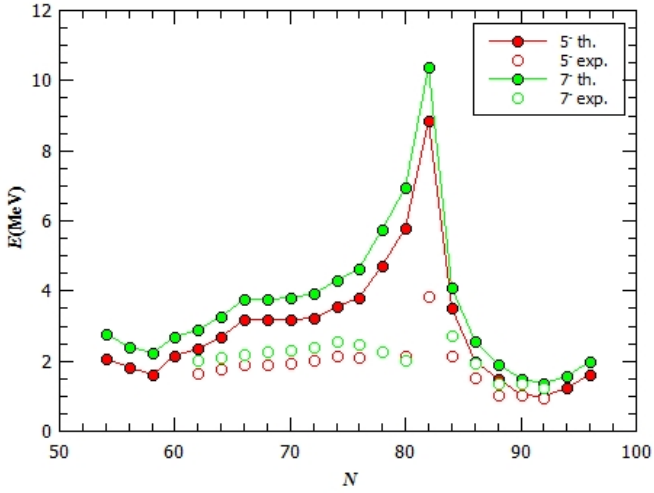

(c) Ba

Figure 3.19: Excitation energies E of states 5^- and 7^- as functions of the neutron number N for Kr, Xe and Ba isotopes.

3.5 Transition strengths

Transition strengths were calculated for $E1$ ($1^- \rightarrow 0^+$), $E2$ ($2^+ \rightarrow 0^+$) and $E3$ ($3^- \rightarrow 0^+$) transitions from the first 1^-, 2^+ and 3^- excited states to the 0^+ ground-state. Calculated transition strengths were expressed in Weiskopff units (W.u.). All transition strengths were plotted as functions of N for Kr, Xe and Ba isotopes. No experimental data was found for B(E1) transition strengths, which is expected since these values are very small, usually $B(E1) < 10^{-2}$ W.u., and not many 1^- states were experimentally observed. Some data was found for $B(E3)$ transition strengths [35, 36], while most of the available experimental data was found for $B(E2)$ transition strengths [26]. Experimental results are shown on graphs with error bars.

Results for $E1$ transitions are shown in Fig. 3.20. It can be seen from Fig. 3.20 that $B(E1)$ values are very small. Among Kr isotopes, ^{94}Kr has the largest calculated value $B(E1) = 0.008917$ W.u., which means that all transition strengths of Kr isotopes are $< 10^{-2}$ W.u.Xe isotopes have larger $B(E1)$ values than Kr isotopes, with ^{154}Xe having the largest calculated value $B(E1) = 0.040887$ W.u. among Xe isotopes. Ba isotopes have the largest $B(E1)$ values among all the isotopes. The Ba isotope with the largest $B(E1)$ value is ^{124}Ba, with $B(E1) = 0.1208$ W.u.

Results for $E2$ transitions are shown in Fig. 3.21. Calculated transition strengths for Kr are in better agreement with experimental results for larger values of $N \geq 48$ and for $N = 36$, than for values $38 \leq N \leq 48$. This was expected since the calculated excitation energies of the 2^+ state for Kr were mostly not in good agreement with experimental values of those energies, with exceptions for $N = 36$ and $N \geq 54$. Results for Xe isotopes are in better agreement with experimental results, with some exceptions. The best agreement between calculated transition strengths and experimental values can be found among Ba isotopes, which was expected because the best results for excitation energies were found among Ba isotopes.

Results for $E3$ transitions are shown in Fig. 3.22. There are six experimentally determined transition strengths for Kr isotopes, one for Xe isotopes and six for Ba isotopes. None of the experimental values are not in good agreement with calculated results, with the exception of ^{144}Ba and ^{146}Ba, which have a very large margin of error. The fact that there is no good agreement between theory and experiment for these transitions was expected because the available experimental data is for those

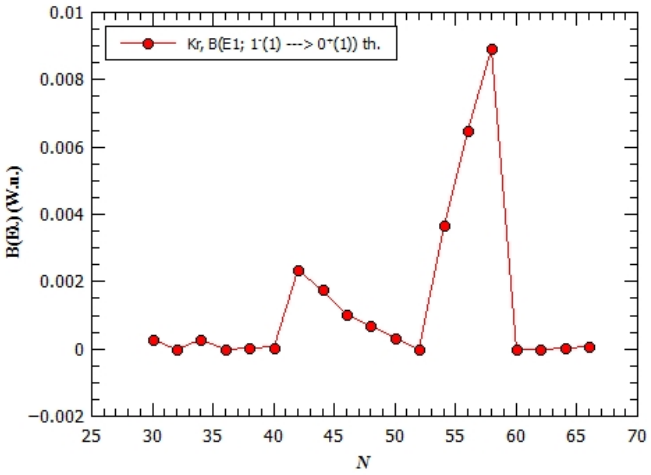

(a) Kr

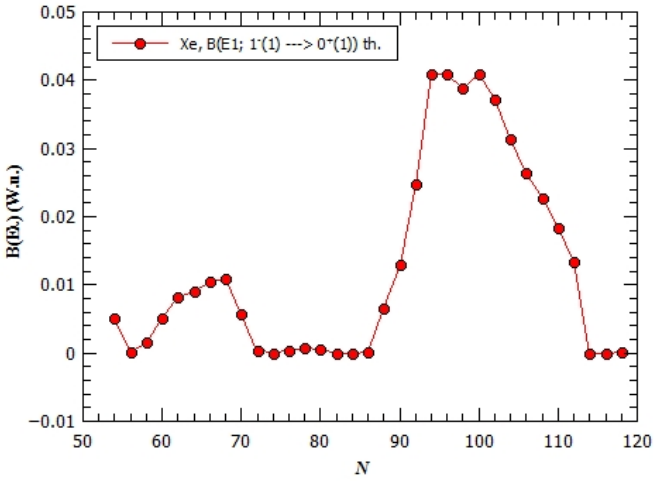

(b) Xe

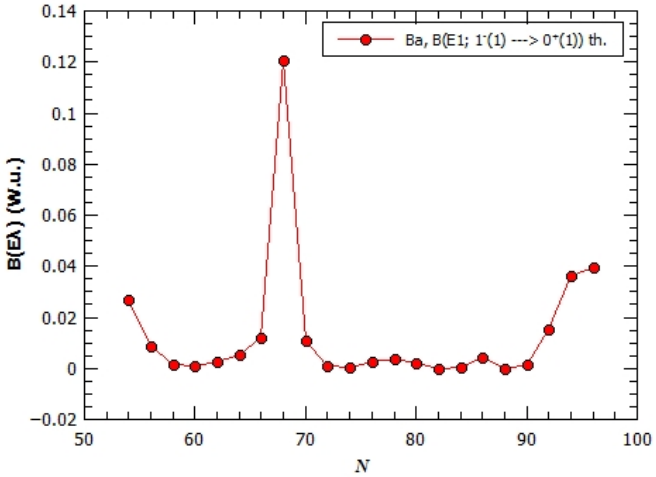

(c) Ba

Figure 3.20: Transition strengths $B(E1; 1^- \rightarrow 0^+)$ as functions of the neutron number N for Kr, Xe and Ba isotopes.

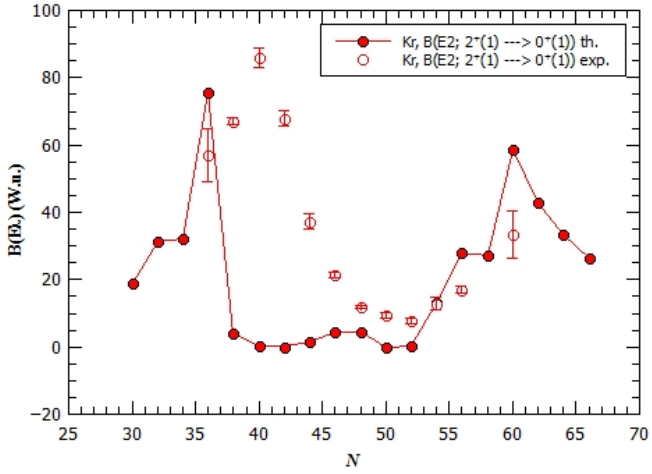

(a) Kr

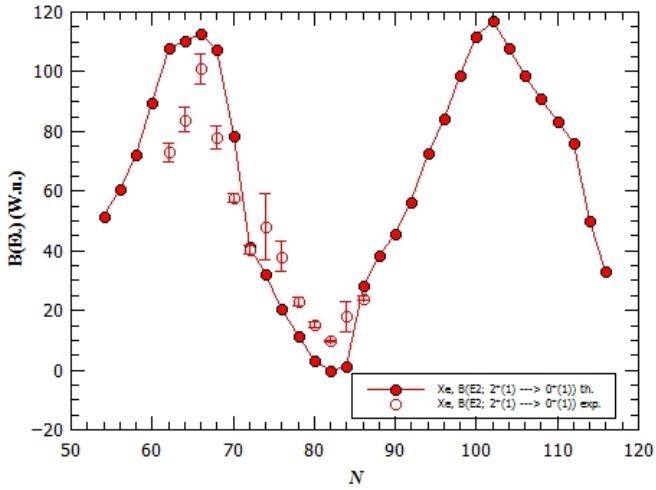

(b) Xe

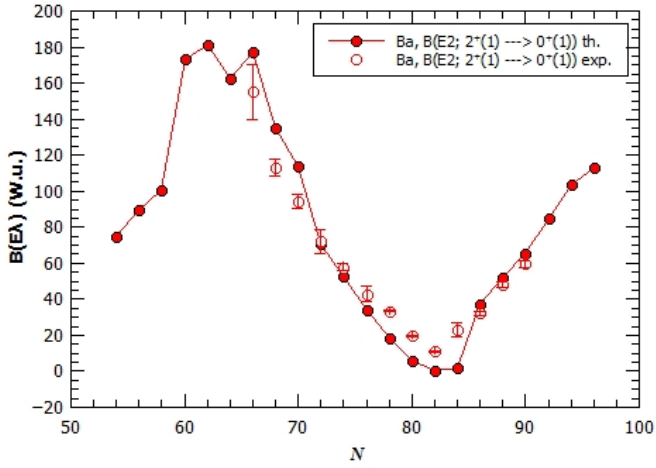

(c) Ba

Figure 3.21: Transition strengths $B(E2; 2^+ \rightarrow 0^+)$ as functions of the neutron number N for Kr, Xe and Ba isotopes.

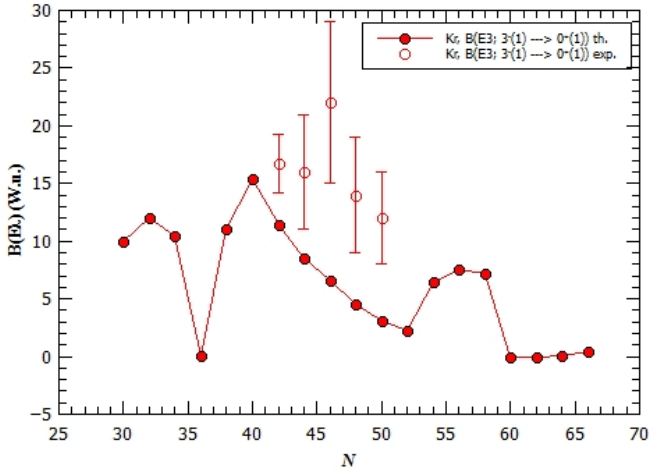

(a) Kr

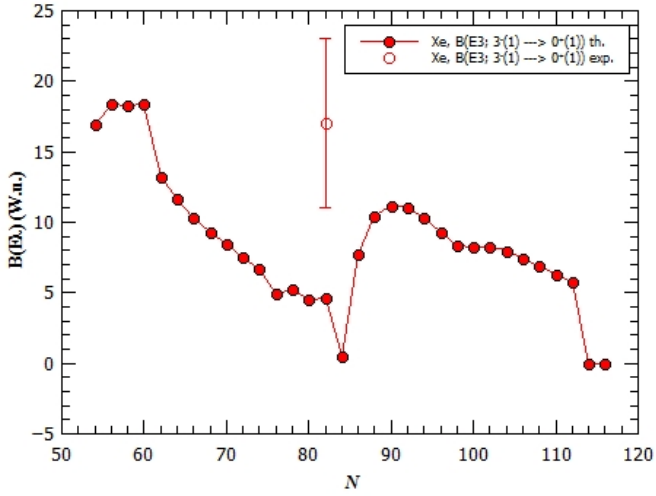

(b) Xe

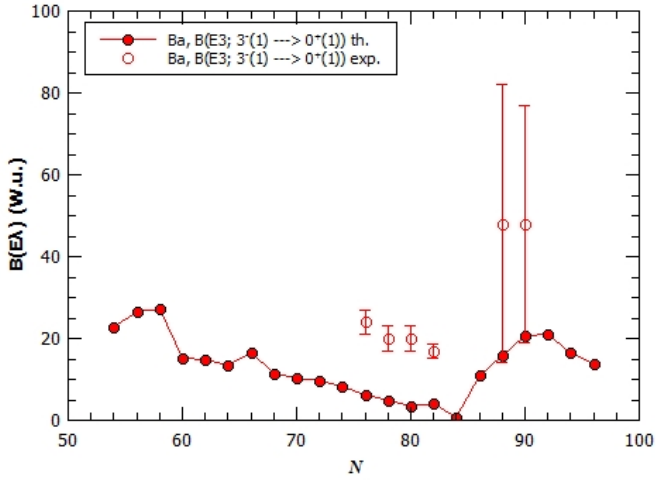

(c) Ba

Figure 3.22: Transition strengths $B(E3; 3^- \to 0^+)$ as functions of the neutron number N for Kr, Xe and Ba isotopes.

nuclei with N close or equal to the magic number 50 or 82, for which the calculated energies of the 3^- state did not show good agreement with experimental results. For those nuclei that are nearly spherical, there is no octupole deformation or octupole softness in the ground-state, so the collective model will not give good results for transition strengths. Octupole deformations were found in ^{144}Ba and ^{146}Ba, so it can be expected that using the collective model will yield good results for transition strengths. While it is true that both of the calculated results are within the margins of error of experimental results, the margins of error of those two isotopes are very large, and more precise measurements in the future will show if there is good agreement between theoretical and experimental results. By including more degrees of freedom, like the triaxial degree of freedom γ, results would be better.

4 Summary and outlook

4.1 Summary

In this work, a formalism of relativistic energy density functionals was used in order to explore quadrupole and octupole correlations in even-even Kr, Xe and Ba isotopes. The DD-PC1 functional was used together with a relativistic Hartree-Bogoliubov model, while low-lying excitation energies and transition strengths were calculated by constructing a quadrupole-octupole collective Hamiltonian. Quadrupole deformations in the ground-state were observed for most nuclei, with the exceptions for nuclei with the magic neutron number 50 or 82 or with the neutron number near the magic number. Octupole deformations were observed in one Kr isotope, one Xe isotope and seven Ba isotopes. Since for Ba isotopes $Z = 56$, this confirmed the empirical knowledge that octupole deformations in the ground-state will be observed more often in nuclei with $N = 34, 56, 88, 134$. Experimental values of binding energies were reproduced with high precision. This confirms that the DD-PC1 functional can be successfully applied to both heavier and lighter nuclei. Calculations were performed for the interval $-0.8 \leq \beta_{2,3} \leq 0.8$ with a step of 0.05. If the step was lower, e.g. 0.01 or 0.02, calculations would be much more time-consuming, but probably more octupole deformations in the ground-state would be observed.

Calculated excitation energies of low-lying 2^+, 4^+ and 6^+ positive-parity states were in good agreement with experimental results for Xe and Ba isotopes, except for nuclei that have a low or no quadrupole deformation in the ground-state, mostly the nuclei with N around or equal to the magic number. The QOCH method did not give good results for Kr isotopes, with some exceptions. One of the reasons for that might be the subshell closure that occurs in ^{76}Kr. Because of that, Kr isotopes with $40 \leq N \leq 50$ have low quadrupole deformations in the ground-state, so the collective model cannot be successfully applied to them. The QOCH method mostly did not give good results for 1^-, 3^-, 5^- and 7^- negative-parity states. This happened because octupole deformations in the ground-state were observed only for some nuclei and many nuclei are not even β_3-soft in the ground-state. This means that for those nuclei, octupole correlations alone cannot be used to describe low-lying negative-parity states and that the energies calculated by the QOCH method will be higher than the experimental ones. Calculated $B(E2)$ transition strengths were in good

agreement with experimental results for Xe and Ba isotopes, while for Kr isotopes, the QOCH method gave good results for isotopes with larger N. Calculated $B(E3)$ transition strengths mostly did not show good agreement with the experimental data, which was expected since the calculated energies of the 3^- state also did not show good agreement with the data. More precise results could be calculated if more degrees of freedom are included. Including the triaxial degree of freedom might improve the results of positive-parity states for Kr isotopes.

4.2 Outlook

Possible further research could be done along the lines presented in this work. The DD-PC1 functional and the QOCH method can be applied to other even-even isotopes. Octupole correlations and deformations in the ground-state could be observed in even-even isotopes of selenium (Se), since it has a proton number $Z = 34$, and in the neighbouring even-even isotopes of germanium (Ge, $Z = 32$). Octupole collectivity could also be observed in even-even isotopes of cerium (Ce, $Z = 58$). A possible improvement of the mean-field calculations and the collective Hamiltonian could be achieved by including the triaxial degree of freedom γ in both the DD-PC1 functional and in the collective Hamiltonian. These new calculations could be applied to even-even isotopes of Kr and, in future research, to even-even isotopes of Se and Ge.

Appendices

Appendix A RHB equations in cylindrical coordinates

In the case of axially symmetric shapes, rotational symmetry is broken and j is no longer a good quantum number, but the densities are still invariant with respect to the rotation around the symmetry axis, here assumed to be the z-axis [31]. Cylindrical coordinates are defined as:

$$x = r_\perp cos\varphi,\ y = r_\perp sin\varphi,\ z. \tag{A.1}$$

The single-particle Dirac spinors $U(\mathbf{r})$ and $V(\mathbf{r})$ are characterized by quantum numbers Ω, π and t, where Ω is the eigenvalue of the symmetry operator J_z, π is the parity and t is the isospin. Spinors can be written as:

$$U(\mathbf{r},s,t) = \frac{1}{\sqrt{2\pi}} \begin{pmatrix} f_U^+(z,r_\perp)e^{i(\Omega-1/2)\varphi} \\ f_U^-(z,r_\perp)e^{i(\Omega+1/2)\varphi} \\ ig_U^+(z,r_\perp)e^{i(\Omega-1/2)\varphi} \\ ig_U^-(z,r_\perp)e^{i(\Omega+1/2)\varphi} \end{pmatrix} \chi_t(t) \tag{A.2}$$

and

$$V(\mathbf{r},s,t) = \frac{1}{\sqrt{2\pi}} \begin{pmatrix} f_V^+(z,r_\perp)e^{i(\Omega-1/2)\varphi} \\ f_V^-(z,r_\perp)e^{i(\Omega+1/2)\varphi} \\ ig_V^+(z,r_\perp)e^{i(\Omega-1/2)\varphi} \\ ig_V^-(z,r_\perp)e^{i(\Omega+1/2)\varphi} \end{pmatrix} \chi_t(t) \tag{A.3}$$

For each solution with positive Ω:

$$\psi_i \equiv \left\{ f_i^+, f_i^-, g_i^+, g_i^-; \Omega_i \right\},\ i = U, V \tag{A.4}$$

there is a time-reversed solution with the same energy:

$$\psi_i = T\psi_i \equiv \left\{ -f_i^+, f_i^-, -g_i^+, g_i^-; -\Omega_i \right\},\ i = U, V. \tag{A.5}$$

Spinors $f_i^{\pm}$ and $g_i^{\pm}$ are expanded in terms of eigenfunctions of a deformed axially symmetric harmonic oscillator potential:

$$V_{osc}(z, r_\perp) = \frac{1}{2}M\omega_z^2 z^2 + \frac{1}{2}M\omega_\perp^2 r_\perp^2. \tag{A.6}$$

Because of volume conservation, oscillator frequencies $\hbar\omega_z$ and $\hbar\omega_\perp$ can be expressed in terms of a deformation parameter β_0 and oscillator frequency $\hbar\omega_0$:

$$\hbar\omega_z = \hbar\omega_0 e^{-\sqrt{5/4\pi}\beta_0},\ \hbar\omega_\perp = \hbar\omega_0 e^{\frac{1}{2}\sqrt{5/4\pi}\beta_0}. \tag{A.7}$$

The corresponding oscillator lengths are defined as:

$$b_z = \sqrt{\hbar/M\omega_z},\ b_\perp = \sqrt{\hbar/M\omega_\perp} \tag{A.8}$$

and because of volume conservation $b_\perp^2 b_z = b_0^3$. The constants β_0 and $\hbar\omega_0$ determine the basis and the eigenfunctions of the deformed harmonic oscillator potential are characterized by quantum numbers:

$$|\alpha\rangle = |n_z, n_\perp, m_l, m_s\rangle\,, \tag{A.9}$$

where n_z and $n_\perp$ represent the number of knots of the wave function in z and $r_\perp$ direction, and m_l and m_s are projections of the orbital angular momentum and spin along the symmetry axis. The eigenvalue of J_z, which is conserved in these calculations is:

$$\Omega = m_l + m_s. \tag{A.10}$$

The parity is determined from the equation:

$$\pi = (-1)^{n_z + m_l}. \tag{A.11}$$

The eigenfunctions of the deformed harmonic oscillator potential are written as:

$$\Phi_\alpha(z, r_\perp, \varphi, s, t) = \phi_{n_z}(z)\phi_{n_\perp}^{m_l}(r_\perp)\frac{1}{\sqrt{2\pi}}e^{im_l\varphi}\chi_{m_s}(s), \tag{A.12}$$

with

$$\phi_{n_z}(z) = \frac{N_{n_z}}{\sqrt{b_z}} H_{n_z}(\xi) e^{-\xi^2/2} \tag{A.13}$$

and

$$\phi^{m_l}_{n_\perp}(r_\perp) = \frac{N_{n_\perp}}{b_\perp} \sqrt{2} \eta^{m_l/2} L^{m_l}_{n_\perp}(\eta) e^{-\eta/2}. \tag{A.14}$$

Parameters ξ and η are given as $\xi = z/b_z$ and $\eta = r^2_\perp / b^2_\perp$, while $H_{n_z}(\xi)$ and $L^m_{n_\perp l}$ are Hermite and Laguerre polynomials defined in [37]. The normalization constants N_{n_z} and $N_{n_\perp}$ are given as:

$$N_{n_z} = \frac{1}{\sqrt{\sqrt{\pi} 2^{n_z} n_z!}},\ N^{m_l}_{n_\perp} = \sqrt{\frac{n_\perp!}{(n_\perp + |m_l|)!}}. \tag{A.15}$$

Spinor components from equations A.2 and A.3 are expanded in the basis of the deformed harmonic oscillator in the following way:

$$f_i(\mathbf{r}, s, t) = \sum_{\alpha}^{\alpha_{max}} f^i_\alpha \Phi_\alpha(\mathbf{r}, s) \chi_{t_i}(t),\ i = U, V \tag{A.16}$$

and

$$g_i(\mathbf{r}, s, t) = \sum_{\alpha}^{\tilde{\alpha}_{max}} g^i_\alpha \Phi_\alpha(\mathbf{r}, s) \chi_{t_i}(t),\ i = U, V. \tag{A.17}$$

In order to avoid spurious solutions, quantum numbers α_{max} and $\tilde{\alpha}_{max}$ are chosen in such a way that the major quantum numbers $N = n_z + 2n_\perp + m_l$ are not larger than $N_{sh} + 1$ for the expansion of small components and not larger than N_{sh} for the expansion of large components [31].

5 Prošireni sažetak

5.1 Uvod

Atomska jezgra je kvantni sustav mnoštva čestica sastavljen od protona i neutrona koji međudjeluju uglavnom putem nuklearne sile, čiji je oblik kompliciraniji od Coulombove sile i gravitacije. Da bi se izbjeglo eksplicitno modeliranje nuklearne sile, razvijeni su različiti modeli. Prema modelu ljusaka, jezgra se može promatrati kao sustav nezavisnih nukleona koji se gibaju u srednjem potencijalu [1]. Energije nukleona su kvantizirane i svaki nukleon popunjava određenu orbitalu (ljusku). Jezgre koje sadržavaju isključivo potpuno popunjene protonske i neutronske ljuske su jače vezane od susjednih jezgara te u osnovnom stanju imaju oblik sfere. Ako je jezgra pobuđena iz osnovnog stanja ili joj je dodano još nukleona, mogu se dogoditi deformacije sferičnog oblika zbog dugodosežnih korelacija između valentnih nukleona [2]. U ovom radu proučavane su kvadrupolne i oktupolne deformacije. Jezgre s osno simetričnom kvadrupolnom deformacijom imaju oblik elipsoida, koji može biti izdužen (oblik lopte za rugby) ili spljošten (oblik diskusa). Jezgre s aksijalno simetričnom oktupolnom deformacijom imaju kruškolik oblik. Oktupolne deformacije su rijeđe od kvadrupolnih i javljaju se kada postoje interagirajuće ljuske suprotnog pariteta čiji se angularni momenti razlikuju za $3\hbar$ [3]. Takve interakcije se uglavnom događaju kod jezgara sa specifičnim protonskim i neutronskim brojevima. Oktupolne deformacije uzrokuju lom refleksijske simetrije. Kod jezgara s jakim oktupolnim deformacijama, javljaju se jake dipolne i oktupolne snage prijelaza. Mjerenje velikih vrijednosti $B(E1)$ snaga prijelaza podrazumijevalo bi narušenje T i CP simetrije [4]. Zbog toga postoji veliki interes za proučavanjem oktupolnih deformacija, te se provode brojni eksperimenti na CERN-u i drugim ustanovama. Pregled najnovijih istraživanja iz tog područja mogu se pronaći u [5, 6].

U ovom radu korišten je samokonzistentni model srednjeg polja (SCMF), u kojem se jezgra promatra kao sustav mnoštva nezavisnih nukleona koji se gibaju u samokonzistentnom potencijalu koji odgovara gustoći raspodjele te jezgre [7–9]. Ovakav model analogan je Kohn-Shamovoj teoriji funkcionala gustoće [10], a jedna od njegovih prednosti je ta problem mnoštva čestica svodi na problem jednog tijela [11]. U modele srednjeg polja spadaju i relativistički modeli srednjeg polja (RMF), u kojima se koriste relativistički energijski funkcionali gustoće (REDF) pri

izračunavanju svojstva jezgre. Formalizam REDF-ova trenutno daje najpotpuniji i najpreciznji okvir za opis svojstava osnovnog stanja jezgara i kolektivnih pobuđenja, te je uspješno primijenjen na jezgre od lakih do superteških, od jezgara u dolini β-stabilnosti do jezgara na granicama doline [12].

Modeli srednjeg polja ne uključuju korelacije sparivanja koje igraju važnu ulogu u jezgrama s otvorenim ljuskama. Pri rješavanju ovog problema primjenjuje se relativistički Hartree-Bogoljubovljev (RHB) model [9, 13]. RHB model pruža jedinstveni opis čestica-šupljina (ph-) i čestica-čestica (pp-) korelacija na razini srednjeg polja koristeći pritom dva srednja potencijala: SCMF potencijal i polje sparivanja [11]. Uvođenjem Bogoljubovljevih kvazičestičnih operatora, osnovno stanje jezgre može se opisati Slaterovom determinantom koja predstavlja vakuum u odnosu na nezavisne kvazičestične operatore.

Još jedan od problema sa SCMF modelom je da dolazi do sloma određenih simetrija, npr. translacijske i rotacijske, zbog čega sam SCMF model ne može biti iskorišten u računu energija pobuđenja i snaga prijelaza. Da bi taj problem bio riješen, SCMF model mora biti proširen, tako da uključuje ponovno uspostavljanje slomljenih simetrija [13]. najčešće korištena metoda je metoda generirajućih koordinata (GCM), koja je veoma uspješna, ali vrlo dugotrajna metoda. U ovom radu korištena je metoda kvadrupolno-oktupolnog kolektivnog hamiltonijana (QOCH) [14, 15], bazirana na REDF formalizmu. U ovoj metodi, vibracijske i rotacijske kinetičke energije su izražene preko parametara deformacije β_2 i β_3 i momenata inercije. Velika prednost ove metode je da izračuni traju svega nekoliko minuta.

Oktupolne deformacije su već dobro proučene za područja od rijetkih zemnih elemenata [16, 17] do lantanoida ($Z \approx 56,\ N \approx 88$) [18, 19] i aktinoida ($Z \approx 88,\ N \approx 136$) [17, 20–23]. Područja s ($Z \approx 34,\ N \approx 34$), ($Z \approx 34,\ N \approx 56$) i ($Z \approx 56,\ N \approx 56$) su manje proučavana pa se u ovom radu posebna pozornost posvećuje upravo njima te se istražuje predviđa li SCMF model oktupolne deformacije za jezgre u tim područjima. Također, istraživanje deformacija u izotopima kriptona bogatim neutronima još je jedna od bitnih tema koja se u novije vrijeme istražuje na CERN-u [24] i RIKEN-u u Japanu [25]. U ovom radu korišten je DD-PC1 funkcional u kombinaciji s RHB modelom. Takav model primijenjen je na parno-pare izotope kriptona ($Z = 56,\ 30 \leq N \leq 66$), ksenona ($Z = 54,\ 54 \leq N \leq 118$) i barija ($Z = 56,\ 54 \leq N \leq 98$). Izračunate su i prikazane površine potencijalnih energija (PES)

u $\beta_2 - \beta_3$ ravnini te su proučavane kvadrupolne i oktupolne deformacije u osnovnim stanjima jezgara, s naglaskom na oktupolne, s obzirom da su one rjeđe. Izračnate su i energije vezanja. Niskoležeće energije pobuđenja su izračunate za stanja do $J^\pi = 7^-$ te su izračunate snage prijelaza između stanja 1^-, 2^+ i 3^- i osnovnog stanja 0^+. Rezultati su uspoređeni s eksperimentalnim podacima, uglavnom sa stranice National Nuclear Data Centera (NNDC) [26]. Rad je organiziran tako da je u drugom poglavlju predstavljen teorijski okvir, u trećem rezultati, a u četvrtom zaključak.

5.2 Teorijski okvir

5.2.1 Kvadrupolne i oktupolne deformacije

Da bi se deformacije jezgre mogle opisati, površina jezgre mora biti parametrizirana na određen način. Jedan od načina je da se površinu opiše razvojem radijvektora u red kuglinih funkcija [3]:

$$R(\theta, \phi) = c(\alpha) R_0 \left[1 + \sum_{\lambda=2}^{\lambda_{max}} \sum_{\mu=-\lambda}^{+\lambda} \alpha_{\lambda\mu} Y^*_{\lambda\mu}(\theta, \phi) \right]. \tag{5.18}$$

R_0 predstavlja radijus sferične jezgre, a $\alpha_{\lambda\mu}$ parametre deformacije. Parametar $c(\alpha)$ određen je iz uvjeta sačuvanja volumena. Da bi radijus bio realan, potrebno je uspostaviti uvjet:

$$(\alpha_{\lambda\mu})^* = (-1)^\mu \alpha_{\lambda-\mu}. \tag{5.19}$$

Dipolni parametri ($\lambda = 1$) određeni su fiksiranjem centra mase tako da za integral po ukupnom volumenu V vrijedi:

$$\int_V \mathbf{r} d^3\mathbf{r} = 0. \tag{5.20}$$

Parametri s $\lambda = 2$ su parametri kvadrupolne deformacije, a parametri s $\lambda = 3$ su parametri oktupolne deformacije. Pretpostavljanjem aksijalne simetrije, iščezavaju svi parametri osim onih s $\mu = 0$. Preostali parametri $\alpha_{\lambda 0}$ uobičajeno su zapisani kao deformacijski parametri β_λ. Oktupolne deformacije nastaju kada postoji interakcija između $(l+3, j+3)$ i (l, j) ljuski suprotnog pariteta. Ovakve interakcije događaju se najčešće kod protonskih i neutronskih brojeva 34, 56, 88 i 134, kao što je prikazano na Slici 2.1.

Kvadrupolne i oktupolne korelacije utječu na izgled niskoležećeg energijskog spek-

tra. Kvadrupolne korelacije uzrokuju spuštanje 2^+ stanja [1], dok su oktupolne korelacije odgovorne za pojavu niskoležećih 1^- i 3^- stanja. Oktupolne korelacije su eksperimentalno potvrđene kod izotopa ^{224}Ra tako što je izmjerena $B(E3; 3^- \rightarrow 0^+)$ snaga prijelaza [2].

5.2.2 Teorija funkcionala gustoće (DFT)

Temeljni postulat DFT računa je taj da se svojstva osnovnog stanja jezgre mogu izraziti preko samo gustoće osnovnog stanja. Time se izbjegava rješavanje Schrödingerove jednadžbe s 3N koordinata jer gustoća $\rho(\mathbf{r})$ ovisi isključivo o tri prostorne koordinate, što jako olakšava račun. Većina DFT računa koristi jednočestične Kohn-Shamove (KS) jednadžbe [10]. Prema Hohenberg-Kohnovom teoremu [27], postoji jedinstveni energijski funkcional:

$$E_s[\rho] = T_s[\rho] + \int d^3r \, v_s(\mathbf{r})\rho(\mathbf{r}), \tag{5.21}$$

takav da je rješenje varijacijske jednadžbe gustoća osnovnog stanja $\rho_s(\mathbf{r})$, pri čemu je $T_s[\rho]$ univerzalni funkcional kinetičke energije neinteragirajućeg sustava, a $v_s(\mathbf{r})$ jedinstveni lokalni jednočestični potencijal. Prema KS shemi, potencijal je takav da se gustoća osnovnog stanja može opisati gustoćom osnovnog stanja neinteragirajućeg sustava:

$$\rho(\mathbf{r}) = \rho_s(\mathbf{r}) = \sum_i^N |\phi_i(\mathbf{r})|^2, \tag{5.22}$$

pri čemu svaka valna funkcija $\phi_i(\mathbf{r})$ takvog sustava za N najnižih popunjenih orbitala zadovoljava KS jednadžbe:

$$[-\nabla^2/2m + v_s(\mathbf{r})]\phi_i(\mathbf{r}) = \epsilon_i\phi_i(\mathbf{r}). \tag{5.23}$$

Za vezani sustav kao što je jezgra, energijski funkcional $F[\rho]$ može se prikazati kao suma kinetičkog funkcionala $T_s[\rho]$, Hartreejevog funkcionala E_H i funkcionala izmjene E_{xc} u kojem su sadržane međučestične interakcije. Potencijal izmjene $v_{xc}[\rho]$ odgovara parcijalnoj derivaciji funkcionala izmjene po gustoći. Na ovaj način, potencijal $v_s[\rho](\mathbf{r})$ može biti zapisan na sljedeći način:

$$v_s[\rho](\mathbf{r}) = v_H[\rho](\mathbf{r}) + v_{xc}[\rho](\mathbf{r}). \tag{5.24}$$

Jednadžbe (5.22), (5.23) i (5.24) rješavaju se samokonzistentno. Funkcional izmjene može se odrediti iz prvih principa nametanjem određenih ograničenja ili prilagodbom na eksperimentalne podatke.

5.2.3 Relativistički model srednjeg polja (RMF)

U RMF modelima, jezgra se promatra kao sustav Diracovih nukleona koji međudjeluju izmjenama mezona i fotona. REDF u ovom radu je konstruiran prilagodbom parametara na empirijske podatke o osnovnim stanjima. Za rješavanje KS jednadžbi, potrebno je konstruirati lagranžijan. Postoje 4 tipa interakcija: izoskalar-skalar: $(\bar{\psi}\psi)^2$, izoskalar-vektor: $(\bar{\psi}\gamma_\mu\psi)(\bar{\psi}\gamma^\mu\psi)$, izovektor-skalar: $(\bar{\psi}\vec{\tau}\psi)\cdot(\bar{\psi}\vec{\tau}\psi)$ i izovektor-vektor: $(\bar{\psi}\vec{\tau}\gamma_\mu\psi)\cdot(\bar{\psi}\vec{\tau}\gamma^\mu\psi)$. Lagranžijan je konstruiran pomoću tri tipa interakcije, bez izovektor-skalar interakcije:

$$\begin{aligned}\mathcal{L} =&\bar{\psi}(i\gamma\cdot\partial - m)\psi \\ &- \frac{1}{2}\alpha_S(\hat{\rho})(\bar{\psi}\psi)(\bar{\psi}\psi) - \frac{1}{2}\alpha_V(\hat{\rho})(\bar{\psi}\gamma^\mu\psi)(\bar{\psi}\gamma_\mu\psi) - \frac{1}{2}\alpha_{TV}(\hat{\rho})(\bar{\psi}\vec{\tau}\gamma^\mu\psi)(\bar{\psi}\vec{\tau}\gamma_\mu\psi) \\ &- \frac{1}{2}\delta_S(\partial_\nu\bar{\psi}\psi)(\partial^\nu\bar{\psi}\psi) - e\bar{\psi}\gamma\cdot A\frac{(1-\tau_3)}{2}\psi.\end{aligned} \tag{5.25}$$

Parametri α zovu se konstante vezanja. Variranjem lagranžijana po $\bar{\psi}$, dobije se jednonukleonska Diracova jednadžba, koja je relativistički analogna jednadžba KS jednadžbi:

$$\left[\gamma_\mu(i\partial^\mu - \Sigma^\mu - \Sigma_R^\mu) - (m + \Sigma_S)\right]\psi = 0, \tag{5.26}$$

pri čemu parametri

$$\Sigma^\mu = \alpha_V(\rho_v)j^\mu + e\frac{1-\tau_3}{2}A^\mu \tag{5.27}$$

$$\Sigma_R^\mu = \frac{1}{2}\frac{j^\mu}{\rho_v}\left\{\frac{\partial\alpha_S}{\partial\rho}\rho_s^2 + \frac{\partial\alpha_V}{\partial\rho}j_\mu j^\mu + \frac{\partial\alpha_{TV}}{\partial\rho}\vec{j}_\mu\vec{j}^\mu\right\} \tag{5.28}$$

$$\Sigma_S = \alpha_S(\rho_v)\rho_s - \delta_S\Box\rho_s \tag{5.29}$$

$$\Sigma_{TV}^\mu = \alpha_{TV}(\rho_v)\vec{j}^\mu. \tag{5.30}$$

predstavljaju vlastite energije nukleona. Izoskalarna četverostruja j_μ, izovekstorska četverostruja $\vec{j}_\mu$ i skalarna gustoća ρ_s definirani su kao očekivane vrijednosti sljedećih operatora u osnovnom stanju $|\phi_0\rangle$:

$$j_\mu = \left\langle \phi_0 \left| \bar{\psi}\gamma_\mu\psi \right| \phi_0 \right\rangle = \sum_k v_k^2 \bar{\psi}_k \gamma_\mu \psi_k \tag{5.31}$$

$$\vec{j}^\mu = \left\langle \phi_0 \left| \bar{\psi}\gamma_\mu\vec{\tau}\psi \right| \phi_0 \right\rangle = \sum_k v_k^2 \bar{\psi}_k \gamma_\mu \vec{\tau} \psi_k \tag{5.32}$$

$$\rho_s = \left\langle \phi_0 \left| \bar{\psi}\psi \right| \phi_0 \right\rangle = \sum_k v_k^2 \bar{\psi}_k \psi_k. \tag{5.33}$$

Gustoća ρ_v je nulta komponenta četverostruje j_μ. Valna funkcija ψ_k predstavlja Diracov spinor. Sumiranje se vrši po svim jednočestičnim stanjima pozitivne energije, pri čemu v_k^2 predstavljaju faktore zaposjednuća. Jednadžbe (5.26) - (5.33) rješavaju se samokonzistentno i iterativno. U jednadžbi (5.26) pretpostavi se određen oblik potencijala te se rješavanjem dane jednadžbe dobiju jednočestične valne funkcije. Te funkcije koriste se u jednadžbama (5.31)-(5.33) za konstrukciju novog seta potencijala. Dani postupak ponavlja se dok ne dođe do konvergencije.

Konstante vezanja su parametrizirane preko 9 parametara:

$$\alpha_S(\rho) = a_S + (b_S + c_S x)e^{-d_S x} \tag{5.34}$$

$$\alpha_V(\rho) = a_V + b_V e^{-d_V x} \tag{5.35}$$

$$\alpha_{TV}(\rho) = b_{TV} e^{-d_{TV} x}, \tag{5.36}$$

gdje je $x = \rho/\rho_{sat}$, a ρ_{sat} nukleonska gustoća u području saturacije za simetričnu nuklearnu materiju. Parametri su određeni iz prilagodbe na eksperimentalne podatke [29] te je preko njih konstruiran DD-PC1 funkcional.

5.2.4 Relativistički Hartree-Bogoljubovljev model (RHB)

RMF modeli ne uzimaju u obzir korelacije sparivanja koje igraju važnu ulogu pri opisu jezgara s otvorenim ljuskama. Hartree-Fock-Bogoljubovljev (HFB) model pruža dobar opis takvih korelacija uvođenjem koncepta kvazičestica. Kvazičestični operatori β definirani su preko operatora stvaranja i uništenja $c^\dagger$ i c:

$$\beta_k^\dagger = \sum_l (U_{lk} c_l^\dagger + V_{lk} c_l). \tag{5.37}$$

Sumiranje se vrši preko cijelog konfiguracijskog prostora. Osnovno stanje jezgre $|\Phi\rangle$ predstavljeno je kvazičestičnim vakuumom koji zadovoljava uvjet $\beta_k |\Phi\rangle = 0$ za svaki k u konfiguracijskom prostoru. Matrica gustoće ρ i tenzor sparivanja κ definirani su kao:

$$\rho_{lk} = \left\langle \Phi \left| c_k^\dagger c_l \right| \Phi \right\rangle = (V^* V^T)_{lk} = \rho_{kl}^* \tag{5.38}$$

$$\kappa_{lk} = \langle \Phi | c_k c_l | \Phi \rangle = (V^* U^T)_{lk} = -\kappa_{kl}. \tag{5.39}$$

Energijski funkcional gustoće $E[\rho, \kappa, \kappa^*]$ definiran je kao očekivana vrijednost hamiltonijana u osnovnom stanju jezgre. Hartree-Fockov hamiltonijan h i polje sparivanja Δ definirani su kao:

$$h_{lk}[\rho, \kappa, \kappa^*] = \frac{\partial E[\rho, \kappa, \kappa^*]}{\partial \rho_{kl}} \tag{5.40}$$

$$\Delta_{lk}[\rho, \kappa] = \frac{\partial E[\rho, \kappa, \kappa^*]}{\partial \kappa_{lk}^*}. \tag{5.41}$$

RHB model predstavlja relativističko proširenje HFB modela. RHB jednadžbe zapisane su u sljedećem obliku:

$$\begin{pmatrix} h_D - m - \lambda & \Delta \\ -\Delta^* & -h_D + m + \lambda \end{pmatrix} \begin{pmatrix} U_k(\mathbf{r}) \\ V_k(\mathbf{r}) \end{pmatrix} = e_k \begin{pmatrix} U_k \mathbf{r} \\ V_k(\mathbf{r}) \end{pmatrix}, \tag{5.42}$$

pri čemu je h_D jednonukleonski Diracov hamiltonijan, m masa nukleona, a Δ polje sparivanja. U ph kanalu korišten je DD-PC1 funkcional, a u pp-kanalu modelirana je sila konačnog dosega. Jednadžbe 5.42 rješavane su u cilindričnom koordinatnom sustavu [12, 31]. Rješavanjem RHB jednadžbi može se izračunati samo lokalni minimum na energijskoj površini. Da bi se energija mogla izraziti kao funkcija kolek-

tivne koordinate q, koristi se metoda kvadratičnog ograničenja, koja koristi varijaciju funkcije:

$$\langle H \rangle + \frac{C}{2} \left(\left\langle \hat{Q} \right\rangle - q \right)^2 , \tag{5.43}$$

gdje $\langle H \rangle$ predstavlja ukupnu energiju sustava, $\left\langle \hat{Q} \right\rangle$ je očekivana vrijednost kvadrupolnog ili oktupolnog operatora, a C konstanta krutosti. Na ovaj način, omogućeno je prikazivanje energijske površine u $\beta_2 - \beta_3$ ravnini.

5.2.5 Kvadrupolno-oktupolni kolektivni hamiltonijan (QOCH)

QOCH metoda koristi se za izračunavanje energija niskoležećeg spektra i snaga prijelaza. Radijus iz jednadžbe 5.18 razvijen je u red do $\lambda = 3$. Pobuđenja iz osnovnog stanja opisuju se pomoću kvadrupolnih i oktupolnih kolektivnih koordinata. Vibracijska i rotacijska kinetička energija mogu se izraziti preko parametara β_2 i β_3 i momenata inercije $\mathcal{I}_k$:

$$\mathcal{T}_{\text{vib}} = \frac{1}{2} B_{22} \dot{\beta}_2^2 + B_{23} \dot{\beta}_2 \dot{\beta}_3 + \frac{1}{2} B_{33} \dot{\beta}_3^2, \tag{5.44}$$

$$\mathcal{T}_{\text{rot}} = \frac{1}{2} \sum_{k=1}^{3} \mathcal{I}_k \omega_k^2. \tag{5.45}$$

Parametri B_{22}, B_{23} i B_{33} zovu se maseni parametri i funkcije su deformacijskih parametara β_2 i β_3. Nakon kvantizacije, kolektivni hamiltonijan glasi:

$$\begin{aligned} \hat{H}_{\text{coll}} = & -\frac{\hbar^2}{2\sqrt{\omega \mathcal{I}}} \left[\frac{\partial}{\partial \beta_2} \sqrt{\frac{\mathcal{I}}{\omega}} B_{33} \frac{\partial}{\partial \beta_2} - \frac{\partial}{\partial \beta_2} \sqrt{\frac{\mathcal{I}}{\omega}} B_{23} \frac{\partial}{\partial \beta_3} \right. \\ & - \frac{\partial}{\partial \beta_3} \sqrt{\frac{\mathcal{I}}{\omega}} B_{23} \frac{\partial}{\partial \beta_2} + \frac{\partial}{\partial \beta_3} \sqrt{\frac{\mathcal{I}}{\omega}} B_{22} \frac{\partial}{\partial \beta_3} \\ & \left. + \frac{\hat{J}^2}{2\mathcal{I}} + V_{\text{coll}}(\beta_2, \beta_3), \right. \end{aligned} \tag{5.46}$$

gdje je $\omega = B_{22} B_{33} - B_{23}^2$. Da bi se riješio problem svojstvenih vrijednosti u jednadžbi 5.46, svojstvene funkcije su razvijene u kompletnoj bazi kvadratno integrabilnih funkcija. Za svaki $\mathcal{I}$, baza je definirana kao:

$$|n_2 n_3 I M K\rangle = (\omega \mathcal{I})^{-1/4} \, \phi_{n_2}(\beta_2) \phi_{n_3}(\beta_3) \, |I M K\rangle \, , \tag{5.47}$$

pri čemu su ϕ_{n_2} i ϕ_{n_3} jednodimenzionalne funkcije harmoničkog oscilatora (HO) koje ovise o β_2 i β_3. Za aksijalno deformirane oblike $K = 0$. Kolektivna valna funkcija može se napisati kao:

$$\Psi_{\alpha}^{IM\pi}(\beta_2, \beta_3, \Omega) = e^{-\mu^2\beta^2/2}\psi_{\alpha}^{I\pi}(\beta_2, \beta_3) \left| IM0 \right\rangle , \tag{5.48}$$

pri čemu faktor $e^{-\mu^2\beta^2/2}$ osigurava da će valna funkcija iščeznuti za ($\beta \to \infty$) [32]. Parametar μ zove se parametar baze. Snage multipolnih prijelaza između stanja s različitim angularnim momentima izračunate su prema sljedećoj relaciji:

$$B(E\lambda; I_i \to I_f) = \langle I_i 0 \lambda 0 | I_f 0 \rangle^2 \left| \int d\beta_2 d\beta_3 \sqrt{\omega \mathcal{I}} \psi_i \mathcal{M}_{E\lambda}(\beta_2, \beta_3) \psi_f^* \right|^2 , \tag{5.49}$$

gdje $\mathcal{M}_{E\lambda}(\beta_2, \beta_3)$ označava električni multipolni prijelaz reda λ.

Dinamika kolektivnog hamiltonijana određena je sa sedam parametara: tri masena parametra B, tri momenta inercije $\mathcal{I}_k$ ($k = 1, 2, 3$) i kolektivni potencijal V_{coll}. Maseni parametri i kolektivni potencijal određuju se preko tzv. "cranking" aproksimacije, dok je za izračun V_{coll} potrebno napraviti korekcije na nulto gibanje (ZPE).

5.3 Rezultati

Izračuni su izvršeni uz pomoć dva koda: DIRHB koda [33] i QOCH koda. Pomoću DIRHB koda izračunate su energijske površine u $\beta_2 - \beta_3$ ravnini. Energijske površine izračunate su za sve kombinacije deformacijskih parametara $-0.8 \leq \beta_2 \leq 0.8$, $-0.8 \leq \beta_3 \leq 0.8$ s razlikom od 0.05, čime je uspostavljen izračun 1089 energija za različite kombinacije β_2 i β_3. Promatrane su kvadrupolne i oktupolne deformacije u osnovnom stanju parno-parnih izotopa kriptona (Kr), ksenona (Xe) i barija (Ba) s naglaskom na oktupolne deformacije s obzirom da su one rjeđe. Izračunate su i energije vezanja i energije deformacije. Energije pobuđenja izračunate su za stanja pozitivnog pariteta 2^+, 4^+, 6^+ i drugo 0^+ stanje (0_2^+) te za stanja negativnog pariteta 1^-, 3^-, 5^- i 7^-. Izračunate su i snage prijelaza $B(E1; 1^- \to 0^+)$, $B(E2; 2^+ \to 0^+)$ i $B(E3; 3^- \to 0^+)$. Svi dobiveni rezultati uspoređeni su s dostupnim eksperimentalnim podacima, uglavnom sa stranice NNDC-a [26].

5.3.1 Kvadrupolne i oktupolne deformacije u Kr, Xe i Ba izotopima

Kvadrupolne deformacije u osnovnom stanju primijećene su kod većine izotopa. Primjer izotopa s kvadrupolnom deformacijom i bez oktupolne deformacije u osnovnom stanju je ^{146}Xe, čiji je PES prikazan na Slici 3.1. Energije na skali su dane u MeV-ima. Još jedan primjer kvadrupolno deformirane jezgre u osnovnom stanju je ^{74}Kr (Slika 3.2), dok je ^{78}Kr (Slika 3.3) primjer jezgre koja je sferična u osnovnom stanju. Oktupolne deformacije u osnovnom stanju uočene su u izotopima ^{76}Kr (Slika 3.4), ^{142}Xe (Slika 3.5) i u 7 izotopa Ba. Primjeri su dani za ^{144}Ba (Slika 3.6), ^{112}Ba (Slika 3.7) i ^{114}Ba (Slika 3.8). Podaci o svim jezgrama s uočenim oktupolnim deformacijama u osnovnom stanju dani su u Tablici 3.1. Činjenica da je najviše oktupolnih deformacija u osnovnom stanju uočeno u izotopima Ba ($Z = 56$), poklapa se s dostupnim eksperimentalnim podacima, prema kojima su oktupolne deformacije češće za specifične protonske i neutronske brojeve, među kojima je i broj 56 [3]. S obzirom da su oktupolne deformacije u osnovnom stanju izračunate za izotope ^{112,114}Ba, potvrđeno je da SCMF model predviđa postojanje oktupolnih deformacija u području ($Z \approx 56,\ N \approx 56$).

Parametri deformacije β_2 i β_3 prikazani su na slici 3.9 u ovisnosti o neutronskom broju N za izotope Kr, Xe i Ba. Zbog efekta zatvorene neutronske podljuske kod ^{76}Kr, gdje posljednja dva neutrona u potpunosti popunjavaju ljusku $p_{1/2}$, Kr izotopi između $N = 40$ i magičnog broja $N = 50$ imaju manje deformacije i dva sferična izotopa u osnovnom stanju (^{78}Kr i ^{86}Kr). Xe i Ba izotopi imaju samo po jedan sferičan izotop i u oba slučaja vrijedi $N = 82$, što je magični broj.

5.3.2 Energije vezanja i deformacijske energije

Energije vezanja po nukleonu (E_B/A) prikazane su na Slici 3.10 kao funkcija nukleonskog broja A. Rezultati su uspoređeni s eksperimentalnim podacima [26]. Pokazano je izvrsno slaganje izračunatih E_B/A s eksperimentalnim podacima.

Energija deformacije E_{def} definirana je kao energijska razlika između energije globalnog minimuma i energije sferične jezgre $E_{def} = E_{min} - E_{sph}$. Za jezgre koje su sferične u osnovnom stanju $E_{def} = 0$. Na Slici 3.11 prikazane su E_{def} u ovisnosti o A za izotope Kr, Xe i Ba. Može se vidjeti da su energije deformacije u pravilu manje za jezgre s manjim kvadrupolnim i oktupolnim deformacijama u osnovnom

stanju. Još jedan oblik energije deformacije je energija oktupolne deformacije E_{oct} definirana kao energijska razlika energije globalnog minimuma energije i energije stanja s istim β_2 i $\beta_3 = 0$, $E_{oct} = E_{min}(\beta_2, \beta_3) - E(\beta_2, \beta_3 = 0)$ Iz definicije, vidljivo je da $E_{oct} \neq 0$ samo za izotope s $\beta_3 \neq 0$ u osnovnom stanju. Napravljen je graf ovisnosti E_{oct} o A za izotope Ba i prikazan na Slici 3.12. Slično kao i kod energija deformacija, energije oktupolne deformacije su u pravilu manje za jezgre s manjim oktupolnim deformacijama u osnovnom stanju.

5.3.3 Postavljanje parametra baze

Parametar baze μ iz jednadžbe 5.48 određen je tako da su uzeta dva izotopa, ^{72}Kr i ^{76}Kr, te su njihove energije osnovnog stanja i energije pobuđenja promatrane u ovisnosti o veličini parametra μ. Interval iz kojeg se može uzeti vrijednost parametra baze je onaj unutar kojeg su energije konstantne, tj. neovisne o vrijednosti parametra μ. Energije osnovnog stanja prikazane su na slici 3.13. Stabilnost energije vidljiva je za interval $9 \leq \mu \leq 14$. Proučavane su i energije pobuđenja u ovisnosti o μ. Energije stanja pozitivnog pariteta prikazane su na Slici 3.14, a energije stanja negativnog pariteta na Slici 3.15. Usporedbom svih rezultata uspostavljeno da je interval u kojem su energije stabilne $11 \leq \mu \leq 14$. Uzeta je vrijednost $\mu = 13$, koja pripada i intervalu $8 \leq \mu \leq 15$ koji je izračunat u [32].

5.3.4 Niskoležeći energijski spektar

Osnovno stanje svih proučavanih izotopa je 0^+. Proučavane su energije za stanja pozitivnog pariteta 2^+, 4^+, 6^+ i 0_2^+ te energije stanja negativnog pariteta 1^-, 3^-, 5^- i 7^-. Sve energije prikazane su na grafovima u ovisnosti o neutronskom broju N.

Energije stanja 2^+ i 0_2^+ prikazane su na Slici 3.16, a energije stanja 4^+ i 6^+ na Slici 3.17. Može se vidjeti da kolektivni model ne daje dobre rezultate za stanje 0_2^+. Za ostala stanja pozitivnog pariteta, rezultati su dobri za sve izotope Xe i Ba, osim za one s N u blizini magičnog broja $N = 82$. z Kr izotope, rezultati su dobri za $N = 36$ i $N \geq 56$. Jedan od razloga tomu je zatvaranje neutronske podljuske kod ^{76}Kr ($N = 40$). Kvadrupolne korelacije odgovorne su za nastanak niskoležećih stanja pozitivnog pariteta. Za izotope bez ili s malim kvadrupolnim deformacijama u osnovnom stanju, što vrijedi za Kr izotope s $40 \leq N \leq 50$, kolektivni model neće dati

dobar opis energija stanja pozitivnog pariteta.

Energije stanja 1^- i 3^- prikazane su na Slici 3.18, a na Slici 3.19 prikazane su energije stanja 5^- i 7^-. Eksperimentalni podaci za 1^- stanja su rijetki, no za one koji su izmjereni, slaganje izračunatih i eksperimentalnih podataka je dobro za sve izotope. Energije preostalih stanja negativnog pariteta se kod Xe i Ba izotopa dobro slažu s eksperimentalnim podacima za izotope s $N \geq 86$. Za Kr izotope nema dobrog slaganja između teorije i eksperimenta. Na spektar stanja negativnog pariteta utječu oktupolne korelacije. To znači da će kolektivni model davati dobre rezultate za one izotope s $\beta_3 \neq 0$ ili za one izotope čiji je potencijal mekan u β_3 u osnovnom stanju. To se javlja kod težih Xe i Ba izotopa, ali ne i kod Kr izotopa. Također, moguće je da za Kr izotope, aksijalna simetrija nije dobra pretpostavka te da bi uključivanjem parametra triaksijalne deformacije γ rezultati bili bolji.

5.3.5 Snage prijelaza

Snage prijelaza $B(E1)$, $B(E2)$ i $B(E3)$ prikazane su u ovisnosti o N za sve izotope. Eksperimentalni podaci pronađeni su za $E2$ prijelaze [26] i za neke $E3$ prijelaze [35, 36]. Sve snage prijelaza izražene su u Weiskopffovim jedinicama (W.u.).

$B(E1)$ snage prijelaza prikazane su na Slici 3.20, $B(E2)$ na Slici 3.21 i $B(E3)$ na Slici 3.22. Za $E1$ prijelaze snage su male, uglavnom $< 10^{-2}$ W.u. te za njih nisu dostupni eksperimentalni podaci za usporedbu. Najviše eksperimentalnih podataka bilo je dostupno za $E2$ prijelaze. Rezultati pokazuju dobro slaganje s eksperimentalnim podacima za Xe i Ba izotope. Za Kr izotope, slaganje je lošije, što je i očekivano s obzirom da se ni energije 2^+ stanja za većinu Kr izotopa nisu dobro slagale s eksperimentalnim podacima. Rezultati za $E3$ prijelaze nisu pokazali dobro slaganje s eksperimentalnim podacima. Jedan od razloga je to što su uglavnom dostupni podaci samo za izotope s N u blizini magičnog broja 50 ili 82, a za te izotope kolektivni model ne daje dobre rezultate. Iznimka su podaci za izotope ^{144}Ba i ^{146}Ba, za koje se izračunate snage nalaze unutar srednje pogreške eksperimentalnih rezultata, no problem je u tome što su pogreške prevelike te su potrebna preciznija mjerenja koja bi pokazala slažu li se izračunate snage dobro s izmjerenim snagama.

5.4 Zaključak

U ovom radu, formalizam relativističkih funkcionala gustoće primijenjen je da bi se ispitale kvadrupolne i oktupolne korelacije u parno-parnim jezgrama Kr, Xe i Ba izotopa. Funkcional DD-PC1 iskorišten je u kombinaciji s relativističkim Hartree-Bogoljubljevim modelom, a za izračun energija niskoležećeg spektra konstruiran je kvadrupolno-oktupolni kolektivni hamiltonijan. Kvadrupolne deformacije u osnovnom stanju opažene su kod većine ispitivanih jezgara. Iznimka su bili izotopi s magičnim neutronskim brojem ili jezgre s neutronskim brojem u blizini magičnog. Oktupolne deformacije opažene su kod jednog Kr izotopa, jednog Xe izotopa i sedam Ba izotopa. S obzirom da za Ba izotope vrijedi $Z = 56$, činjenica da je najviše oktupolnih deformacija u osnovnom stanju opaženo upravo kod tih izotopa je u skladu s dostupnim eksperimentalnim podacima, prema kojima su oktupolne deformacije češće kod jezgara s protonskim ili neutronskim brojevima 34,56,88 i 134. Eksperimentalne vrijednosti energija vezanja reproducirane su s izvrsnom točnošću, što potvrđuje primjenjivost DD-PC1 funkcionala na veliki broj jezgara. Izračuni su rađeni za intervale $-0.8 \leq \beta_{2,3} \leq 0.8$ s razlikom od 0.05. Da je razlika u intervalima manja, npr. 0.01 ili 0.02, izračuni bi trajali puno duže, ali bi vjerojatno bilo opaženo više oktupolnih deformacija u osnovnom stanju.

Izračunate energije stanja pozitivnog pariteta 2^+, 4^+ i 6^+ dobro su se slagale s izmjerenim vrijednostima za Xe i Ba izotope, osim za izotope s malim ili nepostojećim kvadrupolnim deformacijama u osnovnom stanju. To su uglavnom bile jezgre s N u blizini magičnih brojeva ili jezgre kojima je N magični broj. QOCH metoda, uz neke iznimke, nije dala dobre rezultate za izotope Kr. Jedan od razloga za to moglo bi biti zatvaranje podljuske kod ^{76}Kr, zbog čega Kr izotopi s $40 \leq N \leq 50$ imaju vrlo niske kvadrupolne deformacije u osnovnom stanju. QOCH metoda uglavnom nije dala dobre rezultate za energije stanja negativnog pariteta. Razlog tomu je to što su oktupolne deformacije u osnovnom stanju zabilježene samo za nekoliko jezgri. Za one jezgre koje nisu oktupolno deformirane u osnovnom stanju niti imaju mekan potencijal u β_3, kolektivni model neće dati dobre rezultate pri opisivanju niskoležećih stanja negativnog pariteta. Za Xe i Ba izotope, izračunate $B(E2)$ snage prijelaza dobro su se slagale s eksperimentalnim vrijednostima, dok su za Kr izotope rezultati uglavnom bili dobri za izotope s većim N. Izračunate $B(E3)$ snage prijelaza uglavnom nisu bile u dobrom slaganju s eksperimentalnim podacima, što je bilo i očekivano, s obzirom

da isto vrijedi i za izračunate energije 3^- stanja. Precizniji rezultati bili bi dobiveni da je uključeno više stupnjeva slobode, poput triaksijalnog.

Daljnja istraživanja mogla bi se provesti tako da se DD-PC1 funkcional i QOCH metoda primijene na druge parno-parne izotope. Oktupolne deformacije u osnovnom stanju mogu se ispitati kod izotopa selenija (Se), protonskog broja $Z = 34$, kao i kod susjednih parno-parnih izotopa germanija (Ge, $Z = 32$). Što se tiče težih jezgara, dani formalizam mogao bi biti primijenjen i na izotope cerija (Ce, $Z = 58$). Također, izračuni za Kr mogli bi biti ponovljeni s uključivanjem parametra triaksijalne deformacije γ. Takav formalizam mogao bi biti primijenjen i na Se i Ge izotope.

Bibliography

[1] Heyde, K. Basic ideas and concepts in nuclear physics: an introductory approach. 3rd ed. Bristol and Philadelphia: Institute of Physics Publishing, 2004.

[2] Gaffney, L.P. et al., Studies of pear-shaped nuclei using accelarated radioactive beams.// Nature Vol. 497, (2013).

[3] Butler, P.A., Nazarewicz, W., Intrinsic reflection asymmetry in atomic nuclei.// Reviews of Modern Physics, Vol. 68, No. 2, 0034-6861 (1996).

[4] Engel, J., Ramsey-Musolf, M. J., van Kolck, U. Electric dipole moments of nucleons, nuclei and atoms: The Standard Model and beyond.// Progress in Particle and Nuclear Physics Vol. 71, 21-74 (2013).

[5] Butler, P. A. Octupole collectivity in nuclei.// Journal of Physics G: Nuclear and Particle Physics Vol. 43, 073002 (2016).

[6] Butler, P. A. Pear-shaped atomic nuclei.// Proceedings of Royal Society A Vol. 476, 20200202 (2020).

[7] Bender, M., Heenen, P. H., Reinhard, P. G. Self-consistent mean-field models for nuclear structure.// Reviews of Modern Physics Vol. 75, 0034-6861 (2003).

[8] Robledo, L. M. et al. Mean field and beyond description of nuclear structure with the Gogny force: a review.// Journal of Physics G: Nuclear and Particle Physics Vol. 46, 1361-6471 (2018).

[9] Vretenar, D., Afansjev, A. V., Lalazissis, G. A., Ring, P. Relativistic Hartree-Bogoliubov theory: static and dynamic aspects of exotic nuclear structure.// Physics Reports Vol. 409, 0370-1573 (2004).

[10] Kohn, W., Sham, L. J., Self-Consistent Equations Including Exchange and Correlation Effects.// Physical Review Vol. 140, No. 4A, A1133 (1965).

[11] T. Nikšić, D. Vretenar, P. Ring, Progress in Particle and Nuclear Physics (2011).

[12] Marević, P. Mikroskopski opis oktupolnih pobuđenja u izotopima samarija i gadolinija. Diplomski rad. Zagreb: Prirodoslovno-matematički fakultet, 2015.

[13] Ring, P., Schuck, P. The Nuclear Many-Body Problem, Springer-Verlag, Heidelberg, 1980.

[14] Xia, S.Y., Tao, H., Li, Z.P., Nikšić, T., Vretenar, D. Spectroscopy of reflection-asymmetric nuclei with relativistic energy density functionals.// Physical Review C. Vol. 96, 2469-9985 (2017).

[15] Li, Z.P., Song, B. Y., Yao, J. M., Vretenar, D., Meng, J. Simultaneous quadrupole and octupole shape phase transitions in Thorium// Physical Letters B Vol. 726, 0370-2693 (2013).

[16] Nomura, K., Rodriguez-Guzman, A., Robledo, L. M. Spectroscopy of quadrupole and octupole states in rare-earth nuclei from a Gogny force.// Physical Review C Vol. 92, 014312 (2015).

[17] Nomura, K., Vretenar, D., Nikšić, T., Lu, B.-N. Microscopic description of octupole shape-phase transitions in light actinide and rare-earth nuclei.// Physical Review C Vol. 89, 024312 (2014).

[18] Bernard, R. N., Robledo, L. M., Rodriguez, T. R. Octupole correlations in the ^{144}Ba nucleus described with symmetry-conserving configuration-mixing calculations.// Physical Review C Vol. 93, 061302 (2016).

[19] Rodriguez-Guzman, R., Robledo, L. M., Sarrigurren, P. Microscopic description of quadrupole-octupole coupling in Sm and Gd isotopes with the Gogny energy density functional.// Physical Review C Vol. 86, 034336 (2012).

[20] Robledo, L. M., Bertsch, G. F. Global systematics of octupole excitations in even-even nuclei.// Physical Review C Vol. 84, 054302 (2011).

[21] Nomura, K., Vretenar, D., Lu, B.-N. Microscopic analysis of the octupole phase transitions in Th isotopes.// Physical Review C Vol. 88, 021303 (2013).

[22] Robledo, L. M., Butler, P. A. Quadrupole-octupole coupling in light actinides.// Physical Review C Vol. 88, 051302 (2013).

[23] Agbemava, S. E., Afanasjev, A. V., Ring, P. Octupole deformation in the ground states of even-even nuclei: A global analysis within the covariant density functional theory.// Physical Review C Vol. 93, 044304 (2016).

[24] Albers, M. et al. Evidence for a smooth onset of deformation in the neutron-rich Kr isotopes.// Physical Review Letters Vol. 108, 062701 (2012).

[25] Flavigny, F. et al. Shape evoultion in neutron-rich krypton isotopes beyond $N = 60$: first spectroscopy of ^{98,100}Kr.// Physical Review Letters Vol. 118, 242501 (2017).

[26] National Nuclear Data Center, `https://www.nndc.bnl.gov/`

[27] Hohenberg, P., Kohn, W. Inhomogeneous electron gas.// Phyiscal Review Vol. 136, No. 3B, B864 (1964).

[28] Ginocchio, J. N., Relativistic symmetries in nuclei and hadrons.// Physical Reports Vol. 414, 0370-1573 (2005).

[29] Nikšić, T., Vretenar, D., Ring, P. Relativistic nuclear energy density functionals: Adjusting parameters to binding energies.// Physical Review C 78, 034318 (2008).

[30] Berger, J. F., Girod, M., Gogny, D. Time-dependent quantum collective dynamics applied to nuclear fission.// Computer Physics Communication 63, 365 (1991).

[31] Gambhir, Y. K., Ring, P. and Thimet, A. Relativistic mean field theory for finite nuclei.// Annals of Physics Vol. 198, 132-179 (1990).

[32] Nikšić, T., Li, Z. P., Vretenar D., Prochniak, D., Meng, J., Ring, P. Beyond the mean-field approximation. III. Collective Hamiltonian in five dimensions.// Physical Review C, Vol. 79, 034303 (2019).

[33] T. Nikšić et al. DIRHB - a relativistic self-consistent mean-field framework for atomic nuclei.// Computer Physics Communications (2014).

[34] Bohr, A., Mottleson B. R. Nuclear structure Vol. II: Nuclear deformation, World Scientific Publishing, London, 1975.

[35] Kibedi, T., Spear, R. H. Reduced electric-octupole transition probabilities, $B(E3; 0_1^+ \rightarrow 3_1^-)$ - an update.// Atomic Data and Nuclear Data Tables Vol. 80, 35-82 (2002).

[36] Bucher, B. et al. Direct evidence for octupole deformation in ^{146}Ba and the origin of large E1 moment variations in reflection-asymmetric nuclei.// Physical Review Letters Vol. 118, 152504 (2017).

[37] Arfken, G. B., Weber, H.J. Mathematical methods for physicists. 6th ed. Burlington: Elsevier Academic Press, 2005.